THE GEOLOGICAL SOCIETY OF AMERICA®

Sedimentologic and stratigraphic evolution of the Cacheuta basin: Constraints on the development of the Miocene retroarc foreland basin, south-central Andes

E.K. Buelow[1], J. Suriano[2], J.B. Mahoney[3], D.L. Kimbrough[1], J.F. Mescua[4], L.B. Giambiagi[4], and G.D. Hoke[5]

[1]DEPARTMENT OF GEOLOGICAL SCIENCES, SAN DIEGO STATE UNIVERSITY, SAN DIEGO, CALIFORNIA 92182, USA
[2]INSTITUTO DE GEOCIENCIAS BÁSICAS AMBIENTALES Y APLICADAS (IGEBA, UNIVERSIDAD DE BUENOS AIRES Y CONICET), CIUDAD UNIVERSITARIA PABELLÓN II, INTENDENTE GÜIRALDES 2160, CIUDAD AUTÓNOMA DE BUENOS AIRES, CP C1428EHA, ARGENTINA
[3]DEPARTMENT OF GEOLOGY, UNIVERSITY OF WISCONSIN–EAU CLAIRE, 105 GARFIELD AVENUE, EAU CLAIRE, WISCONSIN 54701, USA
[4]INSTITUTO ARGENTINO DE NIVIOLOGÍA GLACIOLOGÍA Y CIENCIAS AMBIENTALES, EL CENTRO CIENTÍFICO TECNOLÓGICO, PARQUE SAN MARTIN S/N, MENDOZA, 5500, ARGENTINA
[5]DEPARTMENT OF EARTH SCIENCES, SYRACUSE UNIVERSITY, 204 HEROY GEOLOGY LABORATORY, SYRACUSE, NEW YORK 13244, USA

ABSTRACT

Retroarc foreland basins in contractional arc settings contain evidence of temporal and spatial variations in magmatic activity, deformation, and exhumation along the continental margin and serve as excellent recorders of subduction dynamics through time. The Cacheuta basin, northwestern Mendoza Province, Argentina, is situated within the transition zone between the Pampean flat-slab subduction segment north of 33°S and the normal-dipping slab segment of the Southern Volcanic Zone to the south, and it records a detailed history of Andean orogenic exhumation at this latitude. The integration of sedimentologic, stratigraphic, geochronologic, and sediment provenance data from the Cacheuta basin constrains orogenic exhumation patterns and basin evolution during basin development. Cacheuta basin strata record at least a 12 m.y. period of basin evolution (ca. 20 Ma to younger than 7.5 Ma), based on new geochronology. The timing of initial basin subsidence is constrained by the lowermost sample in the Mariño Formation, which yielded a maximum depositional age of 19.2 ± 0.26 Ma, ~4 m.y. earlier than previous interpretations. Conglomerate clast counts, thin section petrography, and detrital zircon analyses, coupled with distinct sedimentologic variations, record progressive orogenic exhumation of the Cordillera Principal, Cordillera Frontal, and Precordillera during early to middle Miocene time. Examination of basinal strata demonstrate that uplift of the Cordillera Principal, Cordillera Frontal, and Precordillera, and simultaneous development of the Cacheuta retroarc foreland basin, in the early to mid-Miocene was the result of contractional deformation and crustal thickening during normal subduction-related orogenic processes and did not result from the development of the flat slab in late Miocene time.

LITHOSPHERE GSA Data Repository Item 2018113 https://doi.org/10.1130/L709.1

INTRODUCTION

The high topography of the Central Andes, with mean elevations of ~4000 m, developed in late Cenozoic time by propagation of east-vergent contractional deformation (Ouimet and Cook, 2010). The Andean margin of South America has been and remains one of the most active subduction boundaries in the world, with convergence rates ranging from ~5 to 15 cm/yr during the Cenozoic (Somoza and Ghidella, 2012). Currently, convergence between the Nazca and South American plate is 8–9 cm/yr, with distinct lateral variations in the dip of the subducting slab along the western margin of the continent (Ramos, 1999). The heterogeneity in the dip angle of the subducting Nazca plate has led to a distinct segmentation of the continental margin into alternating flat- and normal-slab subduction segments (Barazangi and Isacks, 1976; Cahill and Isacks, 1992; Gutscher et al., 2000). This segmentation is thought to be responsible for margin-parallel variations in orogenic evolution and a laterally complex foreland basin system; however, the precise influence of the subducting slab's geometry on upper-crustal architecture is poorly understood. The Andean orogeny is an ideal setting in which to examine the relationships among subduction dynamics, deformation of the upper crust, and subsequent basin evolution.

Retroarc foreland basins represent some of the largest sedimentary depocenters in the world and yield a rich detrital record that can constrain the orogenic evolution of the adjacent convergent margin (DeCelles, 2011; Horton and DeCelles, 2001; Jordan et al., 1993). Stratigraphic analyses of Neogene retroarc basins have provided insight into temporal and spatial variations in magmatic activity, deformation, and exhumation along the associated continental margin (e.g., Damanti, 1993; Jordan et al., 1993, 2001; Jordan, 1995; Zapata and Allmendinger, 1996; Johnson et al., 1986; Horton, 1998; Horton and DeCelles, 1997; Irigoyen et al., 2000; Echavarría et al., 2003; Levina et al., 2014). The objective of this investigation was to improve our understanding of orogenic processes in one of the highest parts of the Andes outside the Altiplano-Puna Plateau through detailed interrogation of the sedimentary record preserved in the Cacheuta basin (Fig. 1). The Neogene Cacheuta retroarc foreland basin is located in the south-central Andes, 30 km west-southwest of the city of Mendoza and adjacent to the Aconcagua fold-and-thrust belt (Irigoyen et al., 2000; Giambiagi et al., 2003a, 2012). The integration of sedimentology, conglomerate clast count data, petrographic analysis, and U-Pb detrital geochronology constrains the sediment provenance, sedimentation rates, and reorganization of the orogenic system during the last 20 m.y. Our

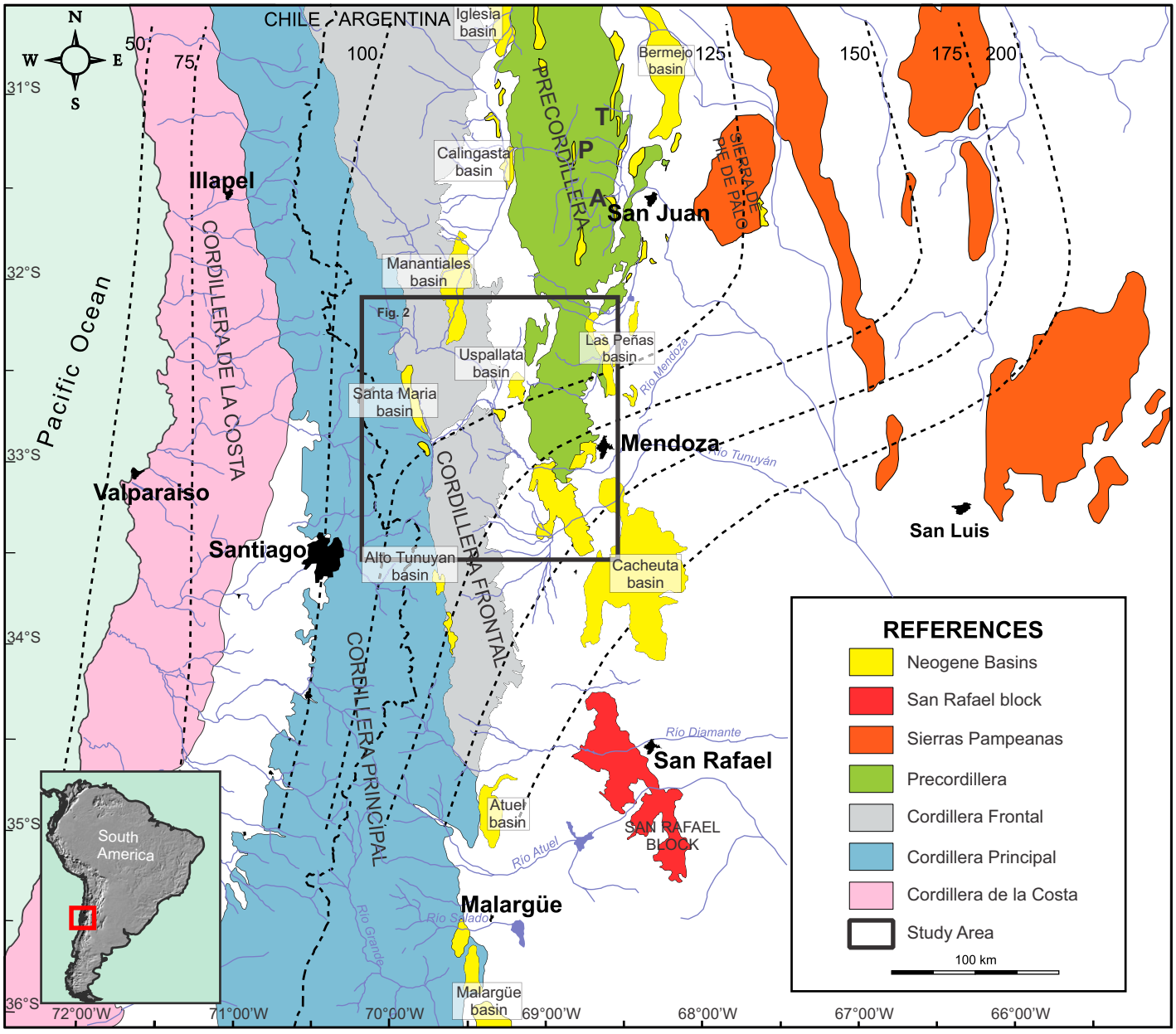

Figure 1. Morphotectonic map of the south-central Andes, which is composed of five distinct morphotectonic provinces, including, from west to east: Cordillera de la Costa, Cordillera Principal, Cordillera Frontal, Precordillera, and Sierras Pampeanas. Neogene basins are shown in yellow. Superimposed dashed lines are depth contours, with depth in kilometers, which illustrate the geometry of the subducting Nazca plate (Cahill and Isacks, 1992). The Cacheuta basin (study area) sits at the transition between the Pampeanas-Chilean flat-slab segment (28–32°30′S) and the normal-subduction segment (south of 33°S; modified from Ramos et al., 2002). T—Talacasto section; P—Pachaco section; A—Albarracín section.

analysis highlights magmatic events and thrust episodicity that constrain the upper-crustal response to subduction dynamics.

GEOLOGIC SETTING

The Cacheuta basin is situated within the transitional zone between the Pampean flat-slab segment to the north and the normal-dipping slab segment of the Southern Volcanic Zone to the south (Fig. 1). The flat-slab region, north of 33°S, is characterized by a lack of syndeformational magmatism, a broad deformational footprint, basement-cored, reverse-faulted block uplifts, and a broken foreland (Jordan et al., 1983; Jordan and Allmendinger, 1986; Astini et al., 2005; Ramos and Folguera, 2009). South of 33°S, the normal-slab region is characterized by active syndepositional magmatism, thin- to thick-skinned fold-and-thrust belts, and a relatively narrow deformational front that migrates episodically and systematically from west to east. These lateral variations in structural style and magmatic activity should be recorded in the derivative detrital record.

The south-central Andes are subdivided into five morphotectonic provinces (west to east): the Cordillera de la Costa, Cordillera Principal, Cordillera Frontal, Precordillera, and the Sierras Pampeanas (Fig. 1). The Cordillera de la Costa underlies the modern forearc and is composed of pre-Andean accretionary belts, Jurassic–Cretaceous volcanic

rocks, and Mesozoic to Miocene calc-alkaline granitoids (Hervé, 1988; Kay et al., 2009). The Cordillera Principal is primarily characterized by thick (5000–6000 m) Jurassic–Cretaceous marine and continental sediments deformed within the Aconcagua fold-and-thrust belt, overlain by Paleogene–Quaternary arc volcanic rocks of the main Andean arc (Figs. 1 and 2; Giambiagi et al., 2003a, 2003b; Ramos et al., 1996; Charrier et al., 2007). The Cordillera Frontal consists of Proterozoic to Devonian metamorphic rocks and late Carboniferous–Early Permian marine sediments and intrusive rocks overlain by the thick (2–4 km) Permian–Triassic rhyolitic succession known as the Choiyoi Group, which dominates the range (Kleiman and Japas, 2009; Sato et al., 2015). To the east, at this latitude, the Precordillera consists of a series of thick-skinned fold-and-thrust sequences of Cambrian–Ordovician carbonate and clastic strata, Devonian turbidite assemblages, Carboniferous to Permian marine strata, and Triassic rift-related sedimentary rocks (Baldis et al., 1984). The Precordillera plunges southward into the subsurface just north of the Neogene Cacheuta basin (Figs. 1 and 2). The easternmost morphotectonic region is the Sierras Pampeanas, which consists of reverse fault block uplifts of Proterozoic to early Paleozoic crystalline metamorphic basement intruded by Paleozoic granitoids (Fig. 1; Jordan and Allmendinger, 1986; Strecker et al., 1989).

PREVIOUS INVESTIGATIONS

Irigoyen et al. (2000) provided the first stratigraphic analysis of the Cacheuta basin and utilized magnetostratigraphy and Ar-Ar geochronology to establish stratigraphic age constraints. Their investigation linked the evolution of the stratigraphic succession to episodes of deformation and volcanism in the Cordillera Principal and Cordillera Frontal and constrained the timing of deformation within the Neogene succession. Irigoyen et al. (2000) inferred that basin subsidence began at ca. 16 Ma in response to a major phase of thrusting in the Aconcagua fold-and-thrust belt in the Cordillera Principal, coincident with eastward migration of the calc-alkaline volcanic axis, both of which were linked to the flattening of the subducting plate.

Structural analysis suggested that uplift and deformation of the Cordillera Principal and development of the Aconcagua fold-and-thrust belt began in the early Miocene (ca. 18 Ma; Giambiagi et al., 2001; Kay et al., 2009; Ramos et al., 1996; Ramos and Folguera, 2009; Siame et al., 2006). At 32°S–33°S, the fold-and-thrust belt consists of a series of north-south–trending faults that propagated east toward the foreland region (Ramos et al., 1996). Development of the Aconcagua fold-and-thrust belt was episodic, with a major contractional phase in the middle Miocene, a quiescent period in the middle to late Miocene, and out-of-sequence thrust

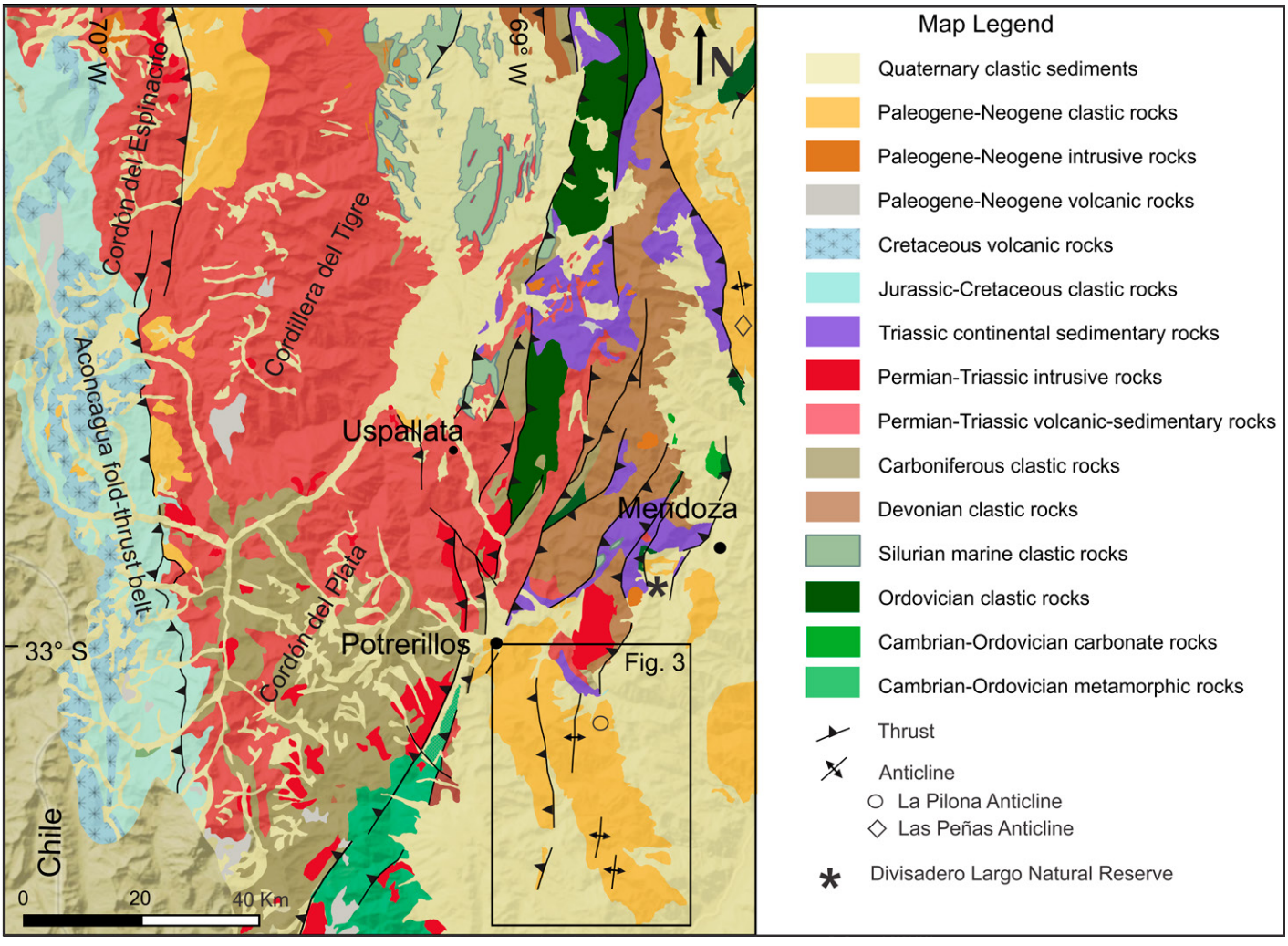

Figure 2. Regional geologic map of the south-central Andes displaying the distribution of geologic units and structures adjacent to the Cacheuta basin. Inset outlines the Cacheuta basin, with detailed geologic map displayed in Figure 3.

reactivation during the late Miocene (Giambiagi et al., 2001). Previous research suggested that late Miocene thrust reactivation was coeval with thick-skinned deformation in the Cordillera Frontal (ca. 9 Ma; Giambiagi et al., 2001; Ramos et al., 2002; Ramos and Folguera, 2009). The onset of deformation in both the Cordillera Frontal and in the Precordillera, however, is not well constrained. North of the study area, the majority of contraction in the Precordillera occurred between 12 and 9 Ma (Allmendinger and Judge, 2014; Levina et al., 2014; Fosdick et al., 2015; Suriano et al., 2017). Late Miocene migration of the eastern deformation front is recorded by reactivation of preexisting faults and thick-skinned deformation of the Sierra Pampeanas metamorphic basement starting at ca. 11–9 Ma (Ramos et al., 2002; Löbens et al., 2013). Eastward migration of the thrust belt was concurrent with the eastward migration of arc magmatism toward the Sierra Pampeanas region, prior to cessation of magmatic activity in late Pliocene time (Kay et al., 2005). The distinct pulse of late Miocene tectonism is interpreted to reflect increased plate coupling during shallowing of the subducting Nazca plate due to impingement of the aseismic Juan Fernandez Ridge (Yáñez et al., 2001; Kay and Mpodozis, 2002; Ramos and Folguera, 2009; Fosdick et al., 2015).

Stratigraphic, geochronologic, and thermochronologic analysis of three foreland basin sections within the Pampean flat-slab segment (31°S –32°S; Talacasto, Pachaco, and Albarracín sections on Fig. 1) suggested that the initial subsidence of the foreland basin began earlier than previously suggested (ca. 24 Ma; Levina et al., 2014). Detrital zircon ages suggest initial uplift of the Cordillera Frontal between 23 and 19 Ma, followed by thrust-induced exhumation of upper Choiyoi Group strata at ca. 17 Ma. Eastward migration of the thrust front into the Precordillera at 14–12 Ma is inferred by an increase in Mesoproterozoic and Paleozoic detrital zircons derived from uplifted Paleozoic strata (Levina et al., 2014). The clustering of apatite (U-Th)/He ages between 12 and 9 Ma across a broad swath of the Precordillera suggests rapid, large-scale exhumation of the Precordillera thrust belt and overlying Cenozoic basin fill at that time (Levina et al., 2014; Fosdick et al., 2015).

CACHEUTA BASIN ANALYSIS

The Cacheuta basin provides critical constraints on orogenic exhumation patterns at 33°S (Figs. 1 and 2). The Cacheuta basin is a Neogene basin, ~25 km N-S and 14 km E-W, containing >2200 m of clastic sediments (Fig. 3). Five formations are present in the basin (Mariño, La Pilona, Tobas La Angostura, Río de los Pozos, and Mogotes; Yrigoyen, 1993) that reflect episodic sediment flux produced during eastward thrust belt propagation (Yrigoyen, 1993; Irigoyen et al., 2000). This investigation combined new field-based sedimentologic and stratigraphic analyses with U-Pb geochronology to provide a refined history of upper-crustal deformation, orogenic exhumation, and basin evolution at the boundary between flat-slab and normal-slab subduction segments at the southern end of the Pampean flat-slab segment of the Central Andes.

Field Work

Cacheuta basin stratigraphy was assessed through the compilation of four stratigraphic sections following the work of Irigoyen et al. (2000; see also Figs. 3 and 4 herein). Thicknesses were determined via measured sections utilizing topographic profiles, structural orientations, and direct measurement. Measured stratigraphic sections provided the framework for collection of sedimentologic data, conglomerate clast counts, petrographic thin sections, volcanic tuff U-Pb geochronology, and detrital zircon (U-Pb) samples. Strata were divided into lithofacies defined by lithologic composition, sedimentary structures, and facies geometry (Figs. 4–7).

Paleocurrent Analysis

Paleocurrent orientations were taken wherever exposure and outcrop orientation permitted accurate measurements. Paleocurrent measurements were taken from imbricated cobbles and channel axes from fluvial channels, foreset laminae from sandy and gravelly bars, and foreset laminae from eolian cross-strata (Fig. 8; Data Repository Table DR1[1]).

Clast Count Analysis

Conglomerate clast composition and textural data were collected at 35 sites throughout the Mariño, La Pilona, Río de los Pozos, and Mogotes Formations to constrain Neogene foreland basin provenance. At each clast count site, 100+ clasts were identified within a 1 m^2 area according to procedures outlined by Howard (1993). Clasts were binned by lithology and size (1–2 cm, 2–3 cm, 3–4 cm, >4 cm; Fig. 9; Table DR2 [see footnote 1]).

Point Count Analysis

Sandstone petrology was evaluated by analysis of 11 thin sections collected from the Mariño, La Pilona, and Río de los Pozos Formations. Point counts were conducted via the Gazzi-Dickinson method (Ingersoll et al., 1984) to constrain sandstone provenance. Results were plotted on compositional and tectonic discrimination diagrams to evaluate stratigraphic trends in sediment provenance (Fig. 10; Table DR3 [see footnote 1]).

Detrital Zircon U-Pb Geochronology

Eighteen zircon geochronology samples were collected from the Cacheuta basin for U-Pb analysis (4 tuff and 14 sandstone samples). Nine of the zircon U-Pb samples were collected from strata within the measured sections, and nine were collected along strike within the basin (see Table DR4 [see footnote 1]). Five of the detrital samples were collected along strike to the north from Mariño and La Pilona outcrops in Potrerillos, Mendoza (Fig. 2). Two of the detrital samples were collected from well-exposed sections of the Río de los Pozos Formation in the Barrancas anticline to the southeast. Two detrital samples were collected from the subjacent Divisadero Largo Formation, one of which came from immediately below the Tosca de Mariño stratigraphic section (Figs. 3 and 4), and one from the Reserva Natural Divisadero Largo to the northeast, in order to constrain the age of the unit (Fig. 2). Sample selection focused on fine- to medium-grained, moderate- to well-sorted sandstone adjacent to major geologic contacts or distinct lithologic transitions and within particularly tuffaceous intervals.

Zircon mineral separation was conducted using conventional crushing and Gemeni table, magnetic, and heavy-liquid separation techniques at the University of Wisconsin–Eau Claire and San Diego State University. Zircons were mounted with epoxy resin alongside Sri Lanka zircon standard SL2 ($^{206}Pb/^{238}U$ age = 564 Ma) and a secondary standard 49127 ($^{206}Pb/^{238}U$ age = 137 Ma). Sample pucks were imaged using a backscattered electron detector (BSE) on a Hitachi S-3400N scanning electron microscope (SEM) at the University of Wisconsin–Eau Claire. Grains were chosen consecutively regardless of size and shape to avoid sampling bias, and care was taken to avoid cracks, inclusions, or grain edges. Zircons were analyzed by laser ablation–inductively coupled plasma–mass spectrometry (LA-ICP-MS) at the University of Arizona LaserChron Center utilizing a

[1]GSA Data Repository Item 2018113, Table DR1A: Cacheuta Basin Paleocurrent Measurements Table 1; Table DR1B: Cacheuta Basin Paleocurrent Measurements; Table DR2: Cacheuta Clast Count Data; Table DR3: Cacheuta Thin Section Modal Analysis; Table DR4: Cacheuta U-Pb Zircon Data, is available at http://www.geosociety.org/datarepository/2018, or on request from editing@geosociety.org.

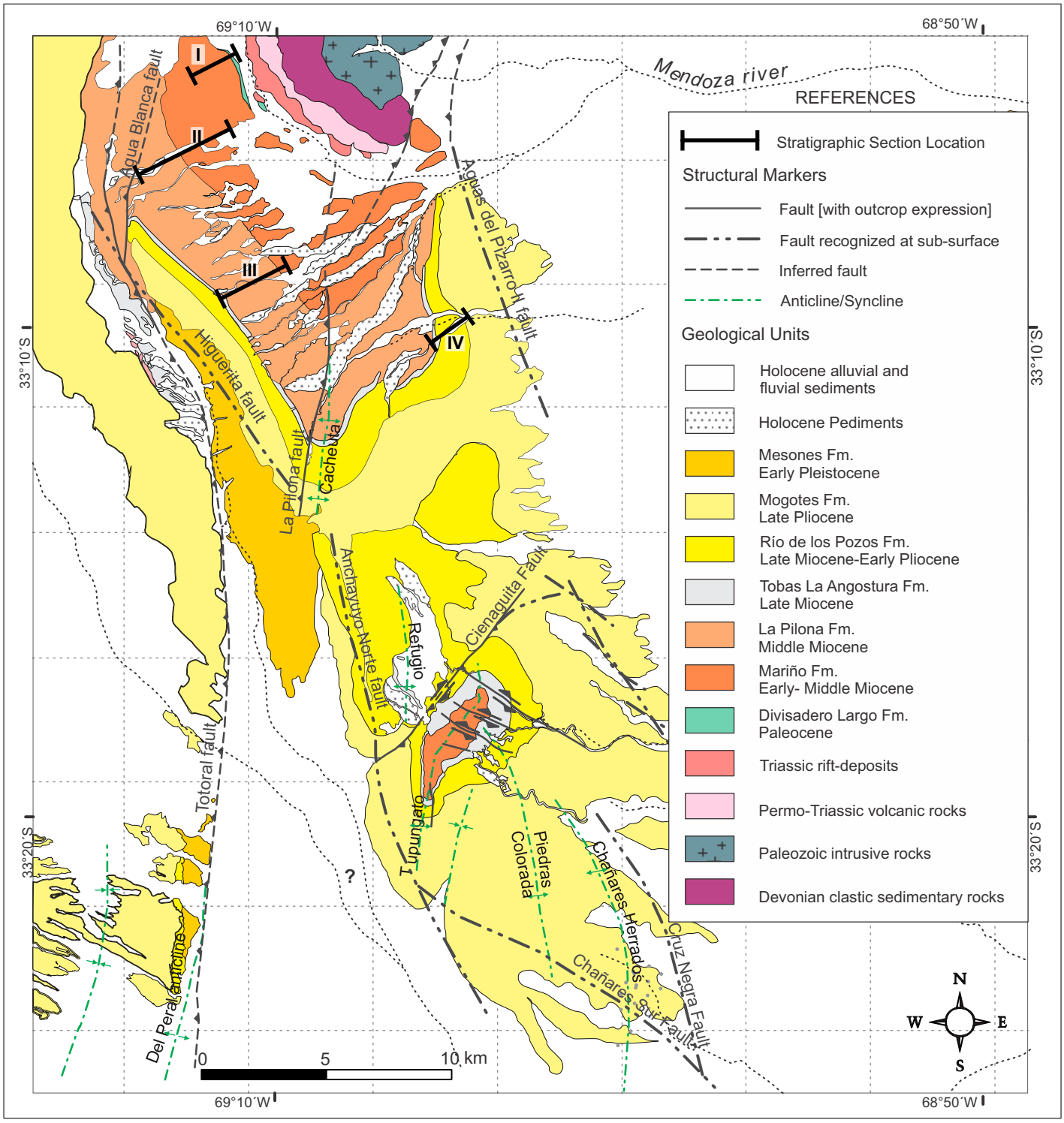

Figure 3. Geologic map of the Cacheuta basin, modified from Giambiagi et al. (2015). Geographic locations are illustrated on Figures 1 and 2. This map displays stratigraphic subdivisions and major structures within the Cacheuta basin. Note locations of four stratigraphic transects used to compile the basin stratigraphy.

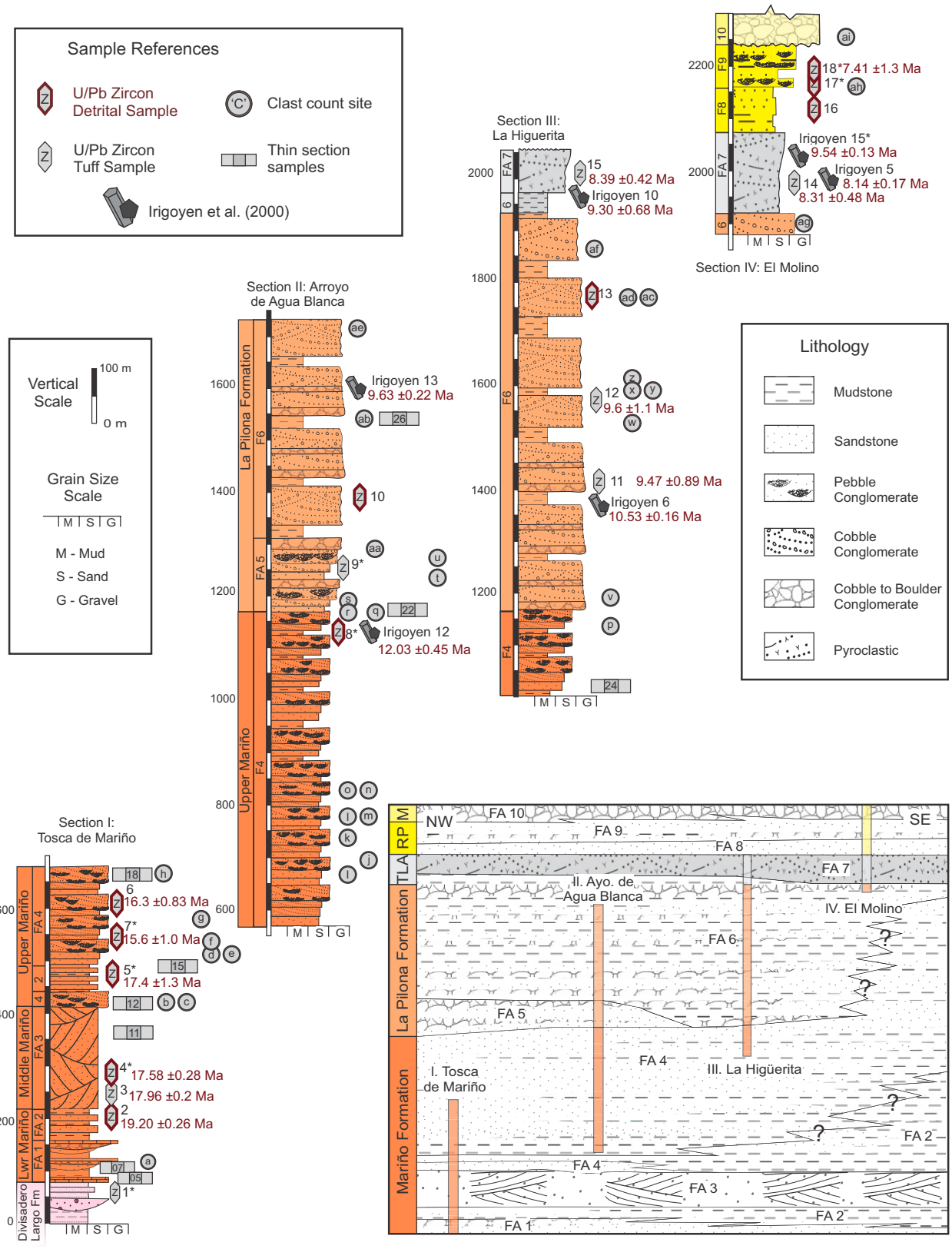

Figure 4. Cacheuta Basin stratigraphy displayed in four measured sections. Sections display lithologic changes in the five units: Mariño, La Pilona, Tobas La Angostura (TLA), Rio de los Pozos (RP), and Mogotes (M). Sections were adopted and extended from sections outlined by Irigoyen et al. (2000). Each section displays the vertical changes in lithology, locations of clast count sites and petrographic and detrital zircon samples, and the maximum depositional ages (MDA) and volcanic tuff U/Pb ages. Inset provides schematic interpretation of the distribution of facies associations across the basin. FA1–10—facies association 1–10.

New Wave DUV193 excimer laser (193 nm) with a spot diameter of 35 µm; methods and procedures were outlined by Gehrels and Pecha (2014). Approximately 100 grains were analyzed from each detrital sample. Interpreted ages were based on $^{206}Pb/^{238}U$ for younger than 900 Ma grains and on $^{206}Pb/^{207}Pb$ for older than 900 Ma grains. Complete U-Pb data tables are provided in Table DR4 (see footnote 1).

Analytical data were plotted on concordia diagrams and age-probability diagrams using the software package Isoplot (Ludwig, 2012). Sedimentary provenance was assessed through the use of normalized probability plots, which facilitated comparison between detrital zircon age peaks and known ages of potential source terranes. Stratigraphic ages were determined utilizing zircon derived from volcanic tuff, with ages calculated using the Zircon Age Extractor (Ludwig, 2012). The maximum depositional age (MDA) of nontuffaceous intervals was determined using the age probability peak of the youngest population of grains ($n \geq 3$) with overlapping ages (Dickinson and Gehrels, 2009; Gehrels, 2014).

RESULTS

Basin Stratigraphy

The Cacheuta basin is divided into five formations: Mariño, La Pilona, Tobas La Angostura, Río de los Pozos, and Mogotes (Figs. 3 and 4; Yrigoyen, 1993; Irigoyen et al., 2000). Stratigraphic correlation of the four measured Cacheuta sections indicates a total stratigraphic thickness of >2240 m (Fig. 4).

The Mariño Formation consists of ~1180 m of intercalated pebble conglomerate, lithic arenite, siltstone, and mudstone, which disconformably overlie the Paleogene Divisadero Largo Formation (section I and II; Figs. 4 and 5A). Initial basin subsidence is indicated by the progradation of the basal Mariño Formation into the gradually subsiding Cacheuta depocenter (Irigoyen et al., 2000).

The La Pilona Formation, observed in sections II, III, and IV, is ~800 m thick and consists of intercalated pebble to cobble conglomerate, lithic arenite, and subordinate fine-grained clastic strata (Fig. 4). There is a marked shift in clast size and composition at the transition from the Mariño Formation to the La Pilona Formation, reflecting a distinct pulse of orogenic exhumation.

The Tobas Angostura Formation consists of ~150 m of recessive, intercalated volcanic tuff and reworked pyroclastic debris, reflecting a pulse of late Miocene volcanism.

The Río de los Pozos Formation is composed of distinctly yellow, poorly consolidated lithic arenite, sandy conglomerate, and multicolored fine-grained clastic sediments. The unit is only clearly exposed in the "El Molino" section (Fig. 4), where it is ~160 m thick. Irigoyen et al. (2000) suggested that the unit varies in thickness across the basin, locally reaching up to 400 m in thickness.

The youngest stratigraphic succession in the Cacheuta basin is the Mogotes Formation, which consists of disorganized pebble to boulder conglomerate. The Mogotes Formation is poorly exposed and difficult to distinguish from overlying unconsolidated Quaternary alluvium. Only an ~10 m section of the unit is exposed in the upper part of section IV (Fig. 4). The total thickness of the Mogotes Formation is unconstrained, but the map pattern suggests the unit is >>100 m thick.

Facies Associations

A facies association is a group of sedimentary facies that are genetically related and therefore represent the basic architectural elements of a particular depositional environment (Walker, 1992). Cacheuta basin strata were subdivided into facies associations based on variations in texture, composition, sedimentary structures, and geometric relationships (Table 1). The distribution of these facies associations is in part stratigraphically controlled, but the facies associations are

TABLE 1. LITHOFACIES OF THE CACHEUTA BASIN

Facies	Descriptions	Depositional environment
FA1	Coarsening-upward sequences (8–20 m) of tabular beds of thinly laminated red siltstone, cross-bedded litharenite, and cross-stratified polymict pebble conglomerate. Contains intercalations of wavy calcrete beds (15–30 cm).	Ephemeral braided fluvial system characterized by periodic high-energy flood events interspersed with quiescent soil development.
FA 2	Coarsening-upward cycles (5–10 m) of medium beds of intraclast-dominated cobble-pebble conglomerate overlain by and medium- to coarse-grained sandstone. Fine-grained red beds are dominated by ripple cross-lamination, mud cracks, raindrop impressions, and bioturbation.	Channel and sheet-flow deposits in prograding lobes (terminal fan or distal megafan environment). Cyclicity resulted from rapid channel migration during episodic high-volume flow.
FA 3	Fine- to medium-grained, well-sorted, litharenite displaying large-scale (1.5–4 m) wedge-shaped cross-stratification.	Eolian dune environment.
FA 4	Cliff-forming coarsening-upward cycles of sandy-conglomerate, lithic arenite, and mudstone. Conglomerate displays stacked, amalgamated lenses with low-angle tangential cross-stratification. Finer beds display soft sediment deformation and water escape structures.	Multistoried nested channels and interchannel mudstone are interpreted as bar and channel sequences of braided stream deposits in a distal terminal fan.
FA 5	Coarsening-upward cycles (10 m thick) of boulder-cobble conglomerate, clast-supported pebble conglomerate, and lithic arenite. Poorly sorted, well-rounded conglomerate is normally graded, lenticular, and contains slightly elongated cross-beds.	Channels and migrating bar deposits in a braided stream environment. Coarsening-upward succession reflects progradation of the braided fluvial system.
FA 6	Stacked lenses of lithic arenite and conglomerate, in a matrix of laminated fine-grained siltstone/mudstone. Lenses are medium to thick bedded, with low-angle erosive scour-and-fill foresets with a basal lag surface.	Braided channels with longitudinal and transverse bars. Abundant sedimentary structures found in finer-grained intervals represent overbank and waning flood deposits.
FA7	Tuff, lapilli tuff, reworked tuff, tuffaceous siltstone, and sandstone beds, with horizontal lamination, normal grading, scour and fill, trough cross-bedding, localized channels, and small- and large-scale trough cross-bedding.	Pyroclastic surge deposits, air-fall, and fluvially reworked pyroclastic debris.
FA8	Recessive, distinctly yellow tuffaceous siltstone to fine sandstone. Medium to thick bedded with thin horizontal lamination and bioturbation. Bedding thickness decreases and bioturbation increases up section.	Unchannelized sheetflood deposits following intermittent volcanism Bioturbation increases up section, suggesting slow sedimentation rates and intermittent quiescence.
FA9	Lenticular channels of clast-supported granule to pebble conglomerate and cross-stratified medium to coarse lithic arenite interbedded with recessive very fine- to medium-grained lithic arenite locally displaying mudstone rip-up clasts and red to green locally tuffaceous siltstone to mudstone. This unit is similar to FA6, but the conglomerate is coarser.	Conglomerate channels and cross-stratified lithic arenite suggest deposition on a distributary braidplain, intercalated with overbank sheetflood and floodplain deposits.
FA10	Lenticular, disorganized, amalgamated cobble to boulder conglomerate beds with minor lenses of very coarse and coarse sandstone lenses.	Proximal alluvial-fan deposit.

laterally and vertically intercalated at a variety of scales throughout the basin (Fig. 4).

Facies Association 1 (FA1)

Facies association 1 (FA1) consists of an ~70-m-thick section of cyclic coarsening-upward sequences (8–20 m) contained within an overall coarsening-upward succession at the base of the Mariño Formation. Each cycle is 8–20 m thick and consists of reddish-brown, thinly bedded, laminated mudstone and siltstone that coarsen upward into light-brown-gray, thin- to medium-bedded, very fine- to fine-grained, litharenite displaying planar cross-stratification (sets ~10–20 cm). The litharenite beds are gradationally overlain by dark-brown-purple, medium- to thick-bedded, trough cross-stratified polymict pebble conglomerate with locally abundant basal rip-up clast horizons. Conglomerate clast size varies from 3 mm at the base to 5 cm at the top of each cycle. Coarsening-upward cycles are interrupted by tabular, laterally continuous, wavy laminated calcrete intervals (15–30 cm; Table 1).

The distinct coarsening-upward cycles, basal rip-up clast horizons, and abundant fine-grained intervals of this facies suggest progradation of braided channelized to unchannelized flows in an alluvial-plain environment (Uba et al., 2005). The normal grading within the reversely graded succession is suggestive of an ephemeral regime, depositing sediments sequentially in high-energy flows during periodic flooding events (Stear, 1985; Reading, 1996; Tucker, 2011). Calcrete intervals represent paleosol horizons developed in ephemeral streams during dry conditions (Reading, 1996; Tucker, 2011; Hoke et al., 2014).

Facies Association 2 (FA2)

Facies association 2 (FA2) contains of a series of fining-upward cycles (5–10 m), each consisting of a basal rip-up clast–dominated conglomerate overlying tabular to lentiform lithic arenite beds, capped by red silty mudstone (Fig. 5B). The intraclastic pebble to cobble (<1–3 cm) conglomerates are clast-supported with trough cross-bedding (sets ~5–10 cm). Lithic arenites are light-pink-tan and medium to coarse grained with sharp to slightly erosive bases. The lithic arenite displays horizontal laminae or low-angle cross-stratification and is locally massively bedded. Fine-grained red beds are thinly bedded (0.5–1 m), with horizontal lamination, ripple cross-lamination, mud cracks, raindrop impressions, and bioturbation (Table 1). The fining-upward cycles are themselves contained within an overall coarsening-upward stratigraphic succession.

Stacked coarsening-upward cycles of tabular beds of rip-up clast conglomerate, tabular to lentiform lithic arenite, and mudstone represent the distributary zone of a sheet-flow–dominated fluvial system (Hampton and Horton, 2007) or a fluvial megafan (Horton and DeCelles, 2001). Lenticular lithic arenite and intraclastic conglomerate represent channel deposits, and tabular lithic arenite represents sheet-flow deposits (Beratan et al., 1999). Mudstone deposits represent overbank deposits. Cyclicity resulted from rapid channel migration during episodic high-volume flow.

Facies Association 3 (FA3)

Facies association 3 (FA3) is characterized by large-scale, trough cross-bedded, fine- to medium-grained, well-sorted lithic arenite with cosets ~1.5–4 m thick (Fig. 5C). The internal composition of the sets alternates from very fine and fine grained to fine and medium grained and locally displays reversely graded laminae (Table 1). Thin-bedded tuffaceous lithic arenite and mud-cracked mudstone are locally intercalated with the trough cross-stratified lithic arenite.

The large-scale cross-bedded lithic arenite is interpreted to be eolian in origin, as suggested by the scale of the trough cross-bedded sets and the internal structures of the laminae (Kocurek and Dott, 1981). The wedge-shaped geometry of the sets indicates barchanoid dune migration (Kocurek and Dott, 1981). Mudstones with mud cracks and horizontally laminated sandstones are interpreted as damp to dry interdune deposits (Kocurek, 1981).

Facies Association 4 (FA4)

Facies association 4 (FA4) is characterized by stacked, amalgamated lenses of conglomerate, well-sorted lithic arenite, and clay beds organized in a cyclical coarsening-upward arrangement (>10 m thick). Red clay beds are thinly laminated and laterally discontinuous and display water escape features. Lithic arenite alternates from lithologically heterogeneous to tuffaceous with abundant soft sediment deformation features. The limited number of fine-grained interbeds locally produces a distinct cliff-forming morphology (Fig. 5E). Pebble-rich lithic arenite is light-gray-tan, medium grained to pebble sized, subrounded to rounded, poorly sorted, and trough cross-stratified. Multicolored clast-supported cobble conglomerate is moderately to poorly sorted, with clasts ranging from 1 to 10 cm in size (average 4 cm; Fig. 5.D). Thick conglomerate beds (0.5–2 m) fine upward and display low-angle tangential trough cross-beds and erosive bases. Even though each cycle is coarsening upward, the overall facies association appears to fine upward, with conglomerate channels that become more isolated and less erosive and transition into scour-and-fill structures upward (Table 1).

The multistoried stacked conglomerate lenses and discontinuous mudstone are interpreted to represent migrating channels and interchannel deposits within a braided fluvial system. Preservation of fine silt and clay beds with localized rip-up clasts reflects cannibalization during channel migration (Steel and Thompson, 1983). The coarsening-upward cycles represent the progradation of feeder channels onto sandy lobes that had previously migrated over a muddy floodplain.

Facies Association 5 (FA5)

Facies association 5 (FA5) is composed of vertically stacked, coarsening-upward sequences (~10 m thick) of lithic arenite, pebble conglomerate, and boulder-cobble conglomerate with minor mudstone interbeds (Fig. 6A). Cobble to boulder polymict conglomerate beds are multicolored, normally graded, and lenticular, with erosive bases, and thick to massively bedded; locally, they display clast imbrication (Fig. 6A). Pebble- to cobble-sized, clast-supported conglomerate is medium to thick bedded, contains well-rounded clasts, and is characterized by stacked, cross-stratified lenticular beds (Fig. 6B). Lithic arenite beds are medium to coarse grained, medium bedded, and tabular and vary from coarse, horizontal lamination to cross-stratified. The scarce fine-grained beds are red and thinly laminated and typically preserve mud cracks.

The vertically stacked, lenticular, normally graded, cobble to boulder conglomerate with sharp erosive bases is interpreted to represent a channel facies in a braided fluvial system. Pebble-cobble conglomerate with planar and low-angle cross-stratification and associated planar stratified lithic arenite are interpreted to represent migrating bar deposits in a braided stream environment (Miall, 1977; Nemec and Steel, 1984). The coarsening-upward succession reflects progradation of the braided fluvial system.

Facies Association 6 (FA6)

Facies association 6 (FA6) consists of stacked lobes of lithic arenite and pebble conglomerate intercalated with thin- to medium-bedded, fine-grained lithic arenite, siltstone, and mudstone in no consistent order (Figs. 6C–6E). Lithic arenite and conglomerate beds are medium to thick bedded, lenticular with erosive bases, and complexly interdigitated. Pebble conglomerate beds are lensoidal and poorly sorted and typically contain basal, locally clast-supported, scour-and-fill structures that grade upward into matrix-supported pebble conglomerate, pebbly lithic arenite, and

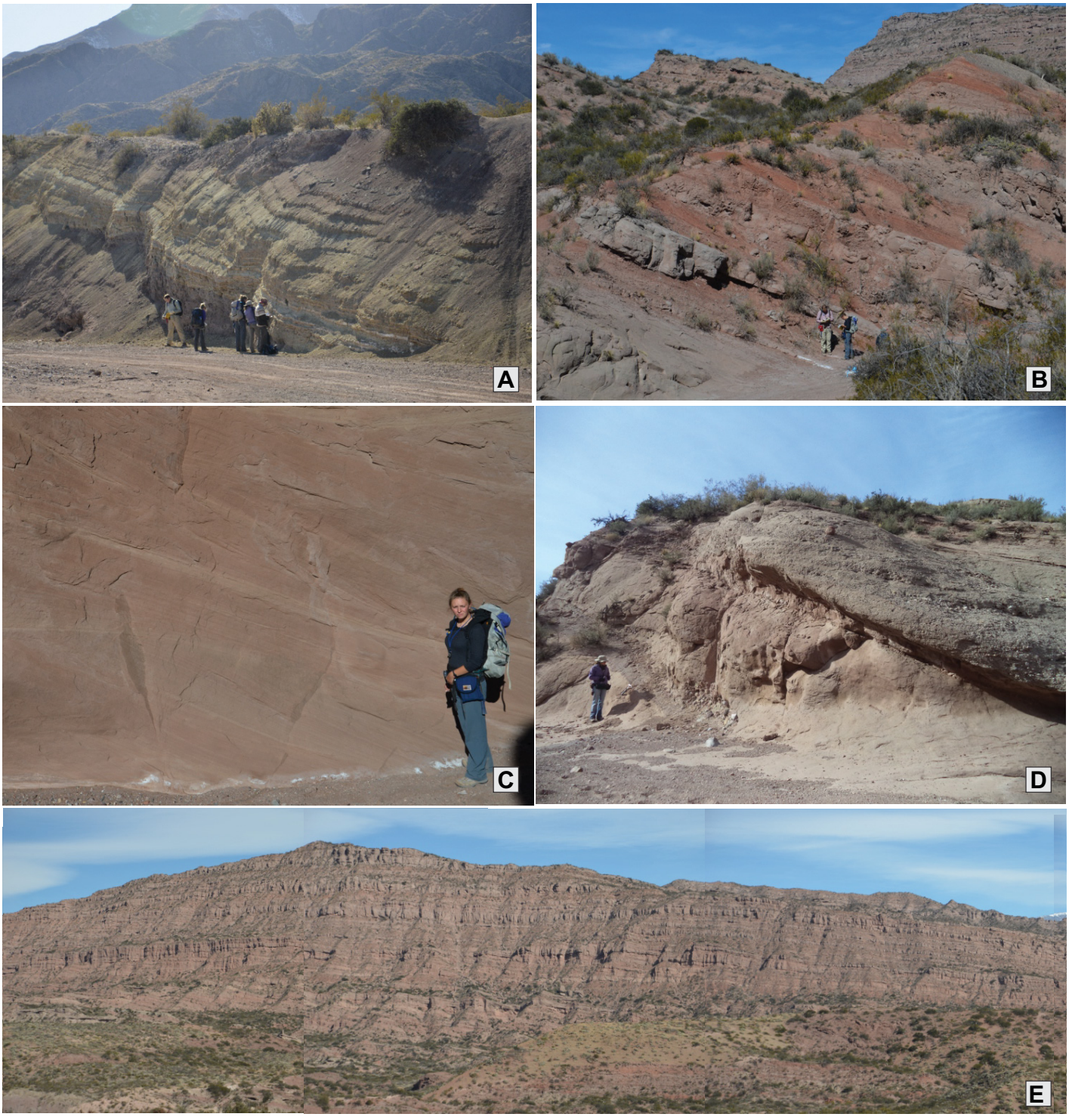

Figure 5. Field photographs of the diagnostic facies of the Divisadero Largo and Mariño Formation facies associations (FA). (A) Divisadero Formation characterized by distinct purple-brown siltstone to sandstone with minor pebble conglomerate, interbedded with green siltstone and fine sandstone. (B) The Mariño FA2 facies is characterized by cycles of red clay and thin-bedded sandstone intercalated with calcrete paleosol horizons. (C) FA3, characteristic of the lower-mid-Mariño facies, is characterized by the thick cross-bedded eolian facies. (D) Contact between the top of the eolian FA3 and the bottom of FA4, characterized by an erosive contact between pebble-cobble channelized bed over dunes and interdunes deposits. (E) The cliff forming Mariño FA4, consisting of repeating coarsening-upward cycles of red silty clay, sandstone, and amalgamated conglomerate channels.

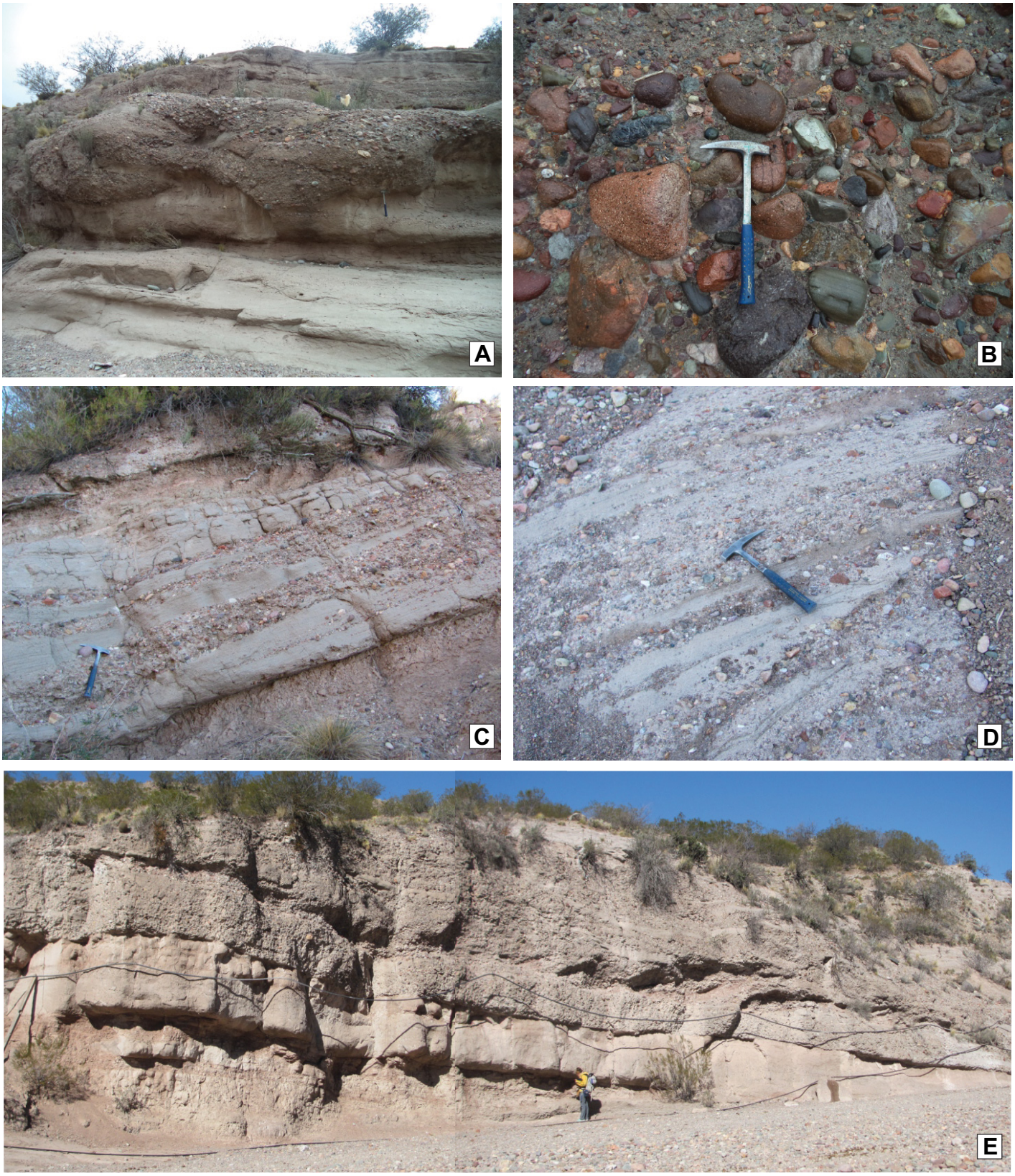

Figure 6. Diagnostic field photographs of the La Pilona Formation facies associations (FA). (A) Erosive Mariño–La Pilona contact. (B) Boulder-cobble conglomerate of FA5. (C) "Typical" facies of the FA6, with stacked lobes of sand, conglomerates, and fines in no consistent order. (D) Detail of conglomeratic bars of FA6 with sandstone interbeds. (E) Coarsening-upward cycles within FA5.

medium- to coarse-grained lithic arenite (Fig. 6D). Sandy lenses vary from medium to coarse lithic arenite to pebbly lithic arenite with shallow scour-and-fill structures evident in coarser-grained intervals. Thin-bedded, fine-grained intervals contain abundant cross-bedding, wavy lamination, and starved ripple structures. Red silty lithic arenite intervals (1–4 m) are recessive and lack sedimentary structures.

The relatively chaotic, complexly interdigitated nature of FA6, with rapid lateral and vertical variations in grain size and sedimentary structures, suggests rapid changes in flow velocity, probably due to episodic discharge events in a medial braidplain system. Periodic high-flow events produce a complexly interfingering system of migrating braided channels with longitudinal and transverse bars and overbank deposits (Bull, 1997; Davidson et al. 2013). The abundant sedimentary structures found in finer-grained intervals represent overbank and waning flood deposits, and thick, structureless siltstone and mudstone may represent overbank slack-water deposits (Miall, 1977). This braided channel belt with interchannel fines could be interpreted as the most proximal sector of the megafan (Horton and De Celles, 2001) or fluvial distributary system (Davidson et al., 2013).

Facies Association 7 (FA7)

Facies association 7 (FA7) is a pyroclastic-rich unit that represents the most abundant and representative facies of the Tobas La Angostura Formation. This facies association is characterized by its recessive weathering pattern and its distinguishing bright light-gray color. It is composed of crystal tuff to lapilli tuff, tuffaceous lithic arenite, and volcanic pebble to cobble conglomerate in medium to thick tabular or lentiforms beds (Fig. 7A). The volcaniclastic-rich beds appears massive but vary from horizontally laminated to trough cross-stratified (Fig. 7B).

The massive to horizontally laminated tuff and lapilli tuff are interpreted as ash fall, while lenticular and parallel to cross-laminated medium tuff to lapilli tuff reflect pyroclastic surge deposits (Fisher and Schmincke, 1984). The volcanic lithic arenite and pebble conglomerate are interpreted as the fluvial reworking of the unconsolidated pyroclastic debris.

Facies Association 8 (FA8)

Facies association 8 (FA8) is only represented in Río de Los Pozos Formation and is characterized by a thinly laminated, poorly consolidated, locally tuffaceous, bright-yellow siltstone to fine-grained lithic arenite lithofacies (Fig. 7C). Bed thickness is difficult to distinguish because of the recessive weathering pattern of the fine-grained material but is generally medium to thick bedded and appears to fine upward. Both thin horizontal laminations and bioturbation are locally evident, with bioturbation increasing up section.

The fine-grained nature, tabular and laterally continuous beds, local tuffaceous character, and horizontal laminations are indicative of unchannelized sheetflood deposits during intermittent volcanism (Irigoyen, 2000). Bioturbation increases up section, suggesting relatively slow sedimentation rates and intermittent periods of quiescence (Olsen, 1987).

Facies Association 9 (FA9)

Facies association 9 (FA9) is very similar to FA6 and is probably a lateral equivalent to that facies association. The unit consists of medium-bedded, lenticular, laterally discontinuous lobes and thin- to medium-bedded, wavy to parallel-laminated beds of fine- to coarse-grained lithic arenite. The sandy beds are intercalated with lenticular channels (~0.5 m thick) of clast-supported granule to pebble conglomerate and cross-stratified medium to coarse lithic arenite. These beds are in part interbedded with recessive, poorly exposed intervals of very fine- to medium-grained lithic arenite locally displaying mudstone rip-up clasts and red to green locally tuffaceous siltstone to mudstone.

The lobate sand beds, lenticular granule to pebble conglomerate channels, and cross-stratified lithic arenite suggest deposition on a distributary braidplain, and the fine-grained, laterally continuous facies represents overbank sheetflood and floodplain deposits (Miall, 1977).

Facies Association 10 (FA10)

Facies association 10 (FA10) is the coarsest and most disorganized lithofacies in the Cacheuta basin. It is composed of multicolored, poorly sorted, clast-supported cobble-boulder conglomerate. The conglomerate forms crude, lenticular amalgamated beds with a massive, disorganized fabric, although clast imbrication and normal grading are locally evident (Fig. 7D). Small lenses (1 m in length and <0.5 m in depth) of matrix-supported cobble conglomerate and sandy lenses are locally interbedded with more massive conglomerate beds. Thin- to medium-bedded, fine-grained lithic arenite, siltstone, and mudstone interbeds are locally evident.

This unit is interpreted to represent deposition in a high-energy environment proximal to a heterogeneous source region. The textural immaturity, clast size, and disorganized fabric of the conglomerate, coupled with the chaotic stacking pattern of the lenticular amalgamated beds, suggest deposition by debris flows, fluidal sediment gravity flows, unchannelized sheetfloods, and channelized stream flows (Nemec and Steel, 1984). This assemblage of depositional mechanisms suggests an alluvial-fan environment characterized by intermittent, high-energy events such as flash floods and gravitational collapse (Blikra and Nemec, 1998).

PALEOCURRENT DATA

Imbricated cobbles and channel axis measurements in the Mariño Formation define a south-southwest–directed (210° to 227°) paleoflow direction, suggesting a source region to the north-northeast (Fig. 8). This geometry is consistent with an orogen-parallel distributary system deriving sediment from the Cordillera Frontal to the north. Measurements from fluvial cross-strata in the Mariño Formation are widely dispersed, with a weak preference for a southwesterly paleoflow, also in agreement with a distributary fluvial system (Fig. 8).

Eolian cross strata from FA2 within the Mariño Formation, although limited, suggest a westerly paleoflow (280°), consistent with a primary wind direction toward the orogenic front.

Paleocurrent data from the La Pilona Formation define an important shift in paleoflow direction. Imbricated cobble orientations describe a mean northeast-directed paleoflow (038°), suggesting exhumation of a source region to the southwest that resulted in a major reorganization of the drainage system. This shift in paleoflow is consistent with a north-to-south migration of the deformational front. Fluvial cross-strata from the La Pilona Formation are limited, but they are suggestive a southwest-directed paleocurrent, suggesting a complex drainage geometry.

PROVENANCE

Conglomerate Clast Composition

Conglomerate clast count data was collected at 35 sites throughout the Cacheuta basin (Fig. 4). Shifts in clast composition are interpreted to reflect shifts in provenance related to eastward propagation of the orogenic wedge and uplift of the different morphotectonic zones. Conglomerates throughout the basin are consistently dominated by rhyolite clasts, making up 43%–92% of the clast compositions (Fig. 9; Table DR3 [see footnote 1]). This indicates that the Cordillera Frontal was a major sediment source throughout the entire time span of deposition in the basin. Other clast lithologies include: andesite, volcanic tuff, phyllite, granitoid,

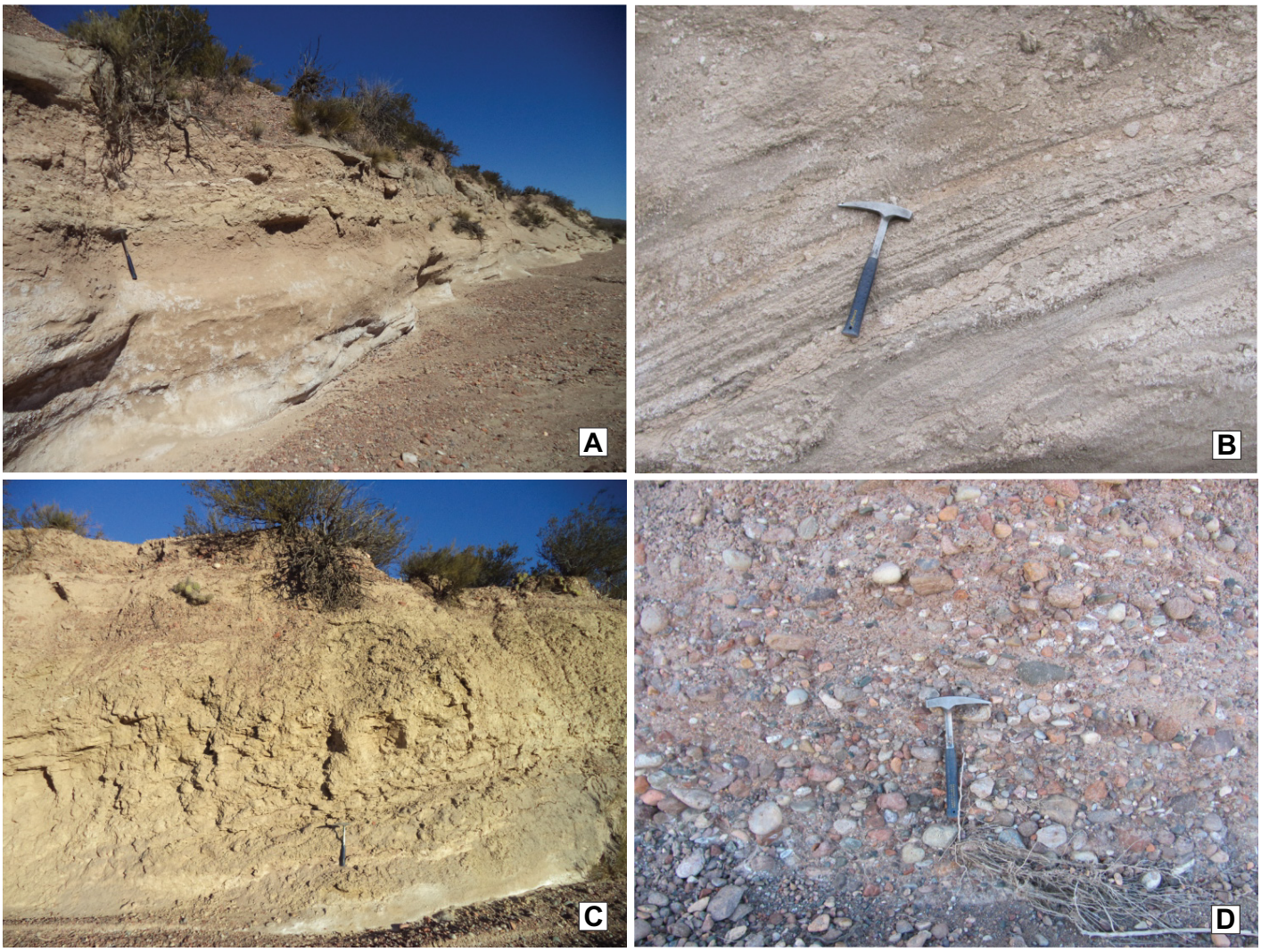

Figure 7. Field images of the Tobas La Angostura, Rio de los Pozos, and Mogotes Formations. (A) General view of Tobas La Angostura Formation. (B) Detail from the distinctly tuffaceous facies association (FA7), which ranges from coarse crystalline tuff to volcanic lithic arenite with tuffaceous intraclasts. (C) Rio de los Pozos FA8, distinguished by bright yellow tuffaceous beds. (D) Detail of Mogotes Formation, characterized by poorly consolidated boulder-cobble conglomerate.

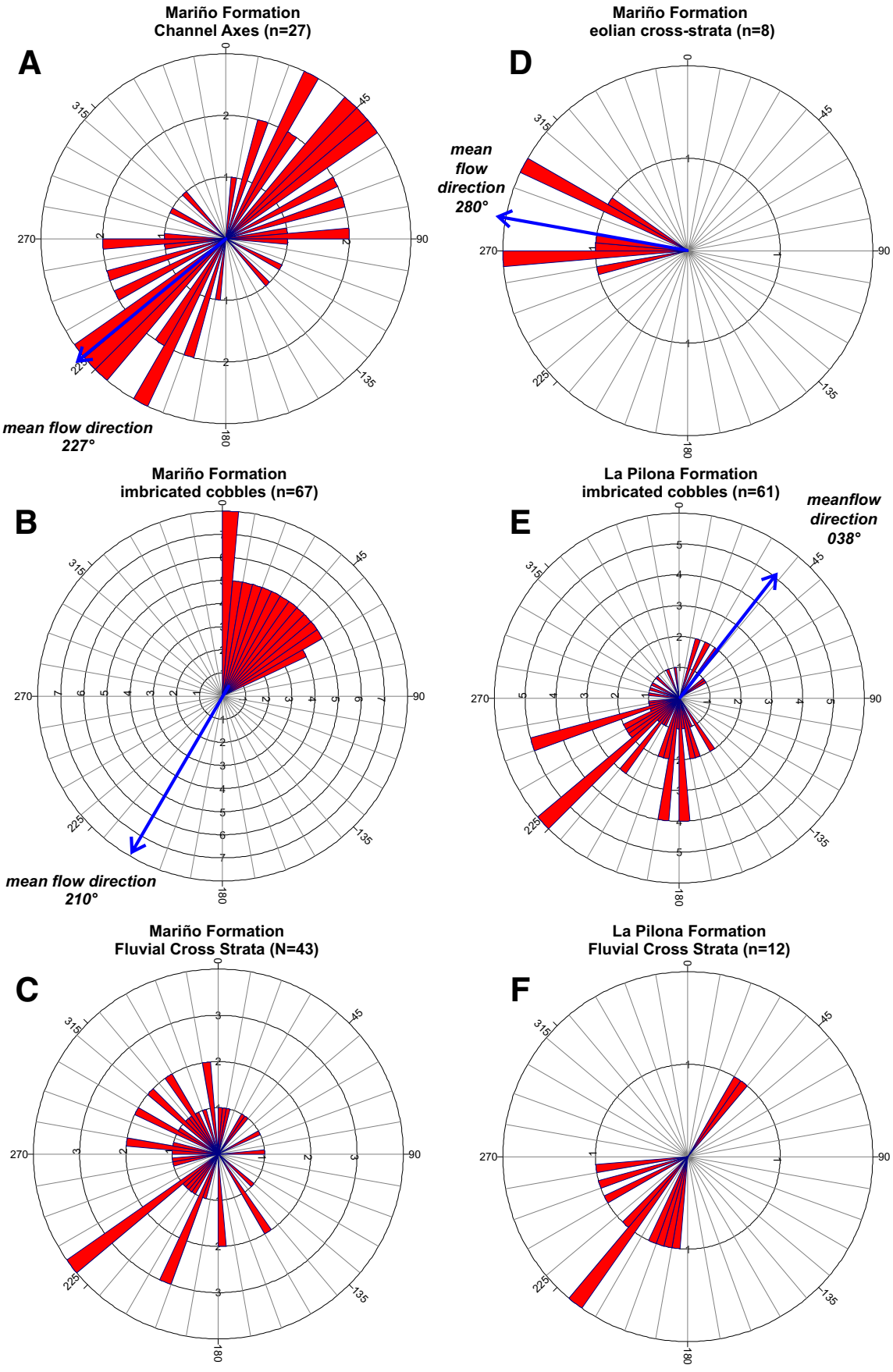

Figure 8. Paleocurrent data from the Cacheuta basin. (A) Channel axes orientations from the Mariño Formation. (B) Imbricated cobble orientations from the Mariño Formation. (C) Foreset laminae from fluvial cross-strata of the Mariño Formation. (D) Eolian cross-strata from facies association 3 (FA3) of the Mariño Formation. (E) Imbricated cobble orientations from the La Pilona Formation. (F) Foreset laminae from fluvial cross-strata of the La Pilona Formation.

quartz, sublithic arenite, red/yellow lithic arenite, green lithic arenite and siltstone, quartzite, metasandstone, and tan micritic to locally fossiliferous limestone clasts. A comprehensive assessment of clast provenance required normalizing clast counts to remove the dominant rhyolite component. While the abundance of rhyolite clasts in the succession is striking, it is worth noting that the durable rhyolite clasts may be preferentially preserved relative to the more labile carbonate or sandstone clasts. Clasts count results were organized stratigraphically to compare compositional shifts throughout the section (Fig. 9).

Sixteen clast count sites were collected in the Mariño Formation (clasts, n = 1946). Rhyolite dominated the clast composition ,representing 66% of the lithology. The remaining 34% of the clasts (n = 654) were normalized and included micritic to fossiliferous limestone (18%), andesite (17%), red lithic arenite (15%), metasandstone (9%), volcanic tuff (12%), green lithic arenite and siltstone (11%), quartz (6%) and quartz arenite (12%). Stratigraphically, andesite, limestone, and red/yellow lithic arenite decrease up section (Fig. 9), and the percentages of rhyolite, quartzite, and metasandstone increase up section, consistent with a transition from an early source in the Cordillera Principal to a more proximal Cordillera Frontal and Precordillera source, as the orogenic front migrated to the east.

Seventeen clast count sites were recorded in La Pilona Formation (n = 2492). The La Pilona Formation conglomerate contains 76% rhyolite clasts. The remaining 24% (n = 593) of the clasts were normalized and included green lithic arenite and siltstone (31%), metasandstone (18%), quartz arenite (13%), andesite (13%), quartz (5%), volcanic tuff (8%), micritic to fossiliferous limestone (6%), granite and phyllite (4%), and red sandstone (2%). The La Pilona–Mariño Formation contact marks a distinct change in nonrhyolite clast lithology (Fig. 9). Andesite, limestone, and red sandstone decrease up section, and there is a distinct increase in green lithic arenite and siltstone relative to the upper Mariño Formation. This increase is interpreted as a result of the uplift of the Precordillera and exposure of the Devonian Villavicencio Formation (Fig. 2).

No clast counts were collected from the Tobas Angostura Formation, which is dominated by volcanic tuff and reworked volcaniclastic sediment. The lack of coarse clastic detritus, the decrease in sedimentation rate, and the basinwide nature of the fine-grained tuffaceous sediment suggest a hiatus in migration of the orogenic front concomitant with a significant pulse of late Miocene volcanism.

Clast compositions of Río de los Pozos and Mogotes Formations were limited to only one clast count site each. The Río de los Pozos Formation, which consists of 79% rhyolite clasts (n = 145), indicated renewed exhumation of Cordillera Frontal sources. The nonrhyolite clasts (n = 31; 21%) were normalized and included green lithic arenite and siltstone (39%), micrite to fossiliferous limestone (23%), andesite (16%), metasandstone (16%), and quartz clasts (6%).

Boulder conglomerate of the Mogotes Formation is dominated by rhyolite (82%; n = 173). The remaining clasts (18%; n = 31) consisted of green lithic arenite and siltstone (45%), micritic to fossiliferous limestone (23%), volcanic tuff (16%), andesite (10%), red lithic arenite (3%), and metasandstone (3%).

Both the Río de los Pozos and the Mogotes Formations are interpreted to be derived primarily from the Cordillera Frontal and Precordillera, consistent with eastward migration of the orogenic wedge.

Clast count trends in the Cacheuta basin record several important compositional shifts. Compositional variations in clast types seem to be temporally controlled and do not appear specific to any particular facies association. First, the distinct increase in rhyolite up section reflects an increasingly important input from the Choiyoi Group of the Cordillera Frontal, starting in the upper portion of the Mariño Formation. Second, there is a distinct increase in green lithic arenite and siltstone up section, starting at the Mariño–La Pilona Formation contact, which is interpreted to represent migration of the orogenic front into the Eastern Precordillera. Third, there is a distinct decrease in micrite to fossiliferous limestone, red lithic arenite, and andesite from the Mariño Formation into the La Pilona Formation, representing a temporal decrease in sediment derived from the Cordillera Principal. Although the data are limited, the reappearance of limestone clasts in the Río de los Pozos and the Mogotes Formations may reflect derivation from early Paleozoic carbonates in the Precordillera or cannibalization of Neogene wedge-top conglomerates in the Cordillera Principal.

Sandstone Petrography

Representative sandstone samples were collected throughout the Cacheuta basin stratigraphy for thin section petrography. Petrography focused on medium-grained lithic arenite to feldspathic arenite. Ten framework grain compositions were recognized, including monocrystalline quartz (Qz), potassium feldspar (Kf), plagioclase feldspar (Pg), volcanic lithic fragments, including felsitic texture (Vr), pumiceous (Vp), microlithic texture (Vi), and lathwork texture (Vb) grains, sedimentary lithic fragments (carbonate [Sc], siliciclastic [Ss]), and low-grade metamorphic lithic fragments, including metasedimentary clasts (Mt). Polycrystalline quartz (Qp) and accessories (As; e.g., zircon, biotite) formed minor components (Table DR3 [see footnote 1]).

Modal thin section analyses from the Cacheuta basin record a distinct petrologic transition that is interpreted to represent shifts in provenance during migration of the fold-and-thrust belt and growth of the orogenic belt (Fig. 10A). The dominance of volcanic lithic fragments throughout the basin results in almost all samples plotting in the undissected to transitional arc field on a tectonic discrimination diagram (Dickinson et al., 1983). Higher-resolution shifts in sediment provenance were elucidated by tracking stratigraphic variations in lithic fragments on a compositional discrimination diagram (Fig. 10B). This diagram discriminates between rhyolitic volcanic lithics (Vr + Vp), intermediate and mafic lithics (Vi + Vb), and metamorphic lithics (Mt), including greenschist-grade metasedimentary clasts (Fig. 10B). Samples from the lower Mariño Formation contained relatively high proportions of intermediate volcanic detritus that was interpreted to be derived from the Cordillera Principal. Sandstone petrology became increasingly felsic upward in the middle Mariño and La Pilona Formations, interpreted to reflect progressive uplift and unroofing of the Cordillera Frontal and western Precordillera, which both provided felsic detritus and diluted sediment supply from the Cordillera Principal (Fig. 10B). The gradual increase in metasedimentary detritus through the upper Mariño Formation and into the La Pilona Formation reflects eastward migration of the fold-and-thrust belt and concomitant unroofing of metasedimentary units of the eastern Cordillera Frontal and the western Precordillera. Enrichment in felsic volcanics (Vr) in the uppermost samples of the upper La Pilona and Río de los Pozos Formations is interpreted to be due to the reactivation of Cordillera Frontal by either structural reactivation or drainage reorganization.

U-Pb Detrital Zircon Provenance

The stratigraphic distribution of detrital zircon U-Pb ages was examined to identify chronological inflection points that would permit the results to be sorted into individual bins useful for provenance analysis (Fig. 11; Table DR4 [see footnote 1]). Individual bins reflect specific source regions within this sector of the Andean orogen (Fig. 11). For example, a prominent Grenville-age peak is interpreted to represent Cuyania and/or Pampean basement, while abundant 240–300 Ma grains are inferred to be derived

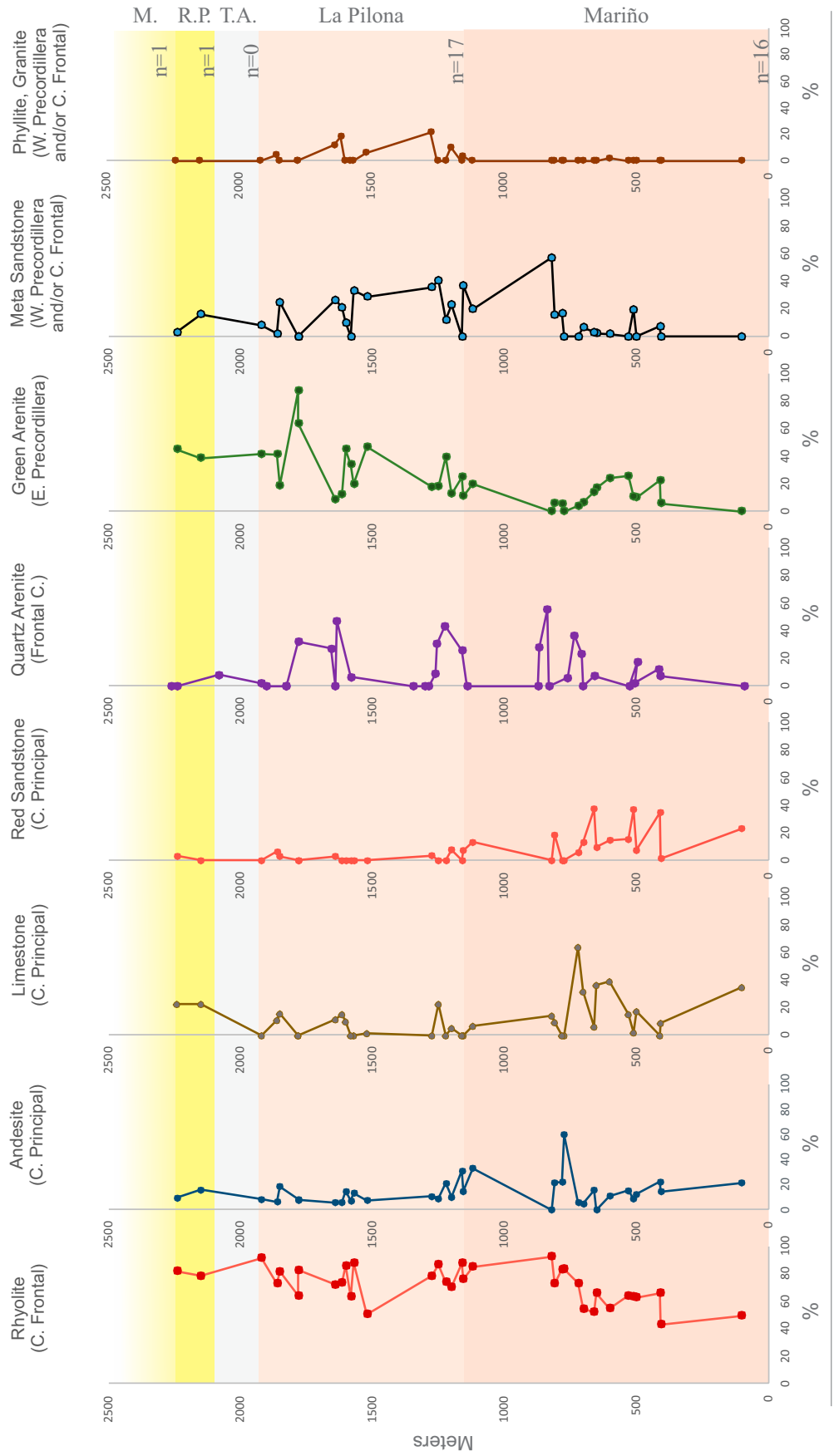

Figure 9. Stratigraphic trends of conglomerate clast composition in the Cacheuta basin. Clast lithologies are characteristic of distinct source regions in the south-central Andes. Circular markers display percent abundance plotted against stratigraphic position of the count. Rhyolite is the dominant clast type, consistently making up 40% or greater of the conglomerate lithologies, and is reported as true percent. The nonrhyolite clasts were normalized after removal of the rhyolite clasts to provide high-resolution analysis of provenance shifts during the evolution of the basin. C.—Cordillera; M.—Mogotes; R.P.—Rio de los Pozos; T.A.—Tobas La Angostura.

Mahoney_L709 3rd pages / 15 of 26

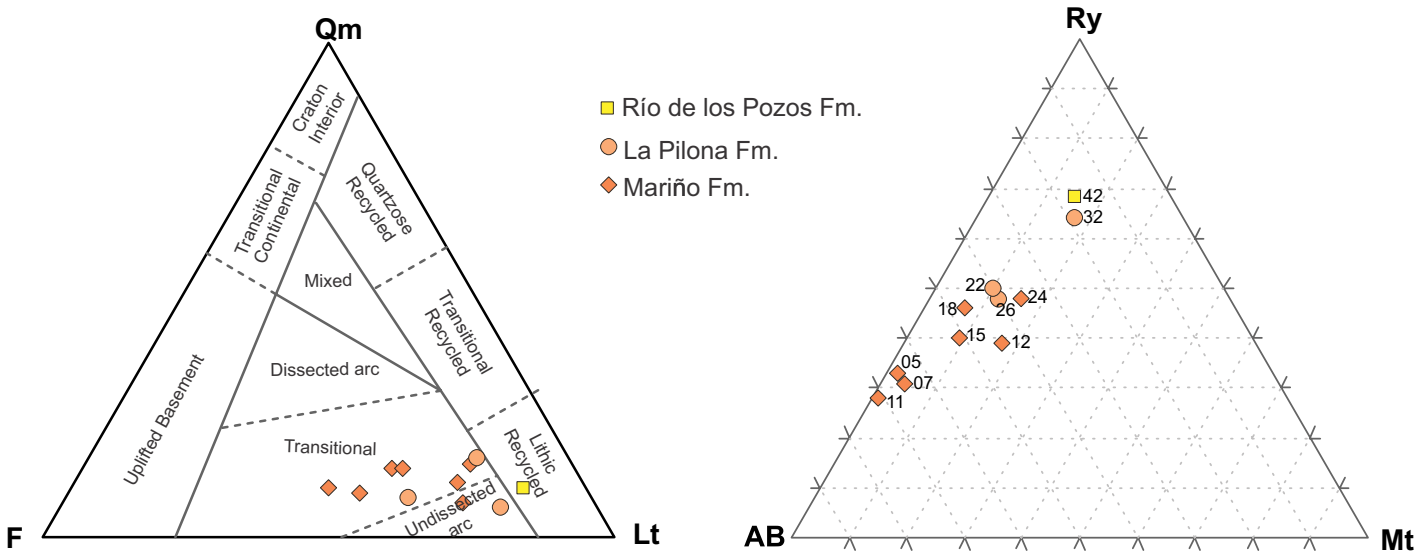

Figure 10. Ternary diagrams illustrating petrographic variations among the Mariño, La Pilona, and Río de los Pozos Formations. (A) Tectonic discrimination diagram (Dickinson et al., 1983) demonstrating that most samples plot in the transitional to undissected fields, due to the high percent of volcanic detritus. Qm—monocrystalline quartz grains, F—feldspar grains, Lt—total lithic grains. (B) Lithics ternary diagram Ry-Mt-AB (Ry—rhyolitic volcanic grains, AB—intermediate and basic volcanic grains, and Mt—metamorphic grains) displaying a distinct trend from 70% AB and <1% Mt to 75% Ry and 15% Mt. This shift reflects the shift in provenance from a predominately Cordillera Principal source in the lower Mariño Formation to Cordillera Frontal in the upper Mariño Formation to Precordillera sources in the La Pilona Formation (for the stratigraphic location of each sample, see Fig. 4).

from the Permian–Triassic Choiyoi magmatic province (Rocha-Campos et al., 2011; Spalletti et al., 2009). There are no grains in the Cacheuta basin age distributions that cannot be accounted for by local Andean sources within the 33°S transect. However, caution is required in provenance interpretations, because it is difficult to differentiate first-cycle detritus from zircon grains recycled from strata younger than the theoretical source region (e.g., Grenville-age grains recycled from Devonian strata). Figure 11 displays the U-Pb zircon age bins, respective ages, and interpreted sources.

Zircon U-Pb results are displayed stratigraphically both by formation (via the pie diagrams) and by individual sample (via the normalized probability plot; Fig. 11). There are several distinct provenance shifts that have important implications for basin evolution (Fig. 11).

The most obvious stratigraphic trend is a steady increase in the percentage of the detrital zircon population derived from the Choiyoi Group of the Cordillera Frontal, which varies from 12% at the base of the Mariño Formation to 47% within the Río de los Pozos Formation. The zircon fertility of the Choiyoi Group is impressive, and, in a manner similar to the conglomerate clasts, it has the potential to swamp the detrital zircon signal from less-productive strata (Capaldi et al., 2017). Therefore, apparent stratigraphic trends in detrital zircon populations should be examined with caution.

There is a notable stratigraphic variation in the percent of Mesoproterozoic zircon, which varies from 9% near the base of the section to a maximum of 24%–25% in the upper Mariño and La Pilona Formations, and then back to 12% in the Río de los Pozos Formation. Early to Middle Paleozoic zircon maintains a relatively steady percentage of ~12%–15% throughout the basinal strata, although it decreases to 7% in the Río de los Pozos Formation. The late Paleozoic detrital zircon population varies from 17% to 20% in the lower portion of the basin, and decreases to 8%–9% in upper basin strata (Fig. 11).

Jurassic to Cretaceous zircon is volumetrically significant (9%) in the lower portion of the Mariño Formation, decreasing steadily to 3%–4% in the La Pilona and Río de los Pozos Formations.

Paleogene zircon comprises 9% of the detrital zircon population in the Mariño Formation at the base of the section, but it decreases to ~1% in the Río de los Pozos Formation at the top of the section. The abundance of Miocene zircon is variable throughout the succession, from a low of 6%–10% in the upper Mariño and La Pilona Formations, to 14%–19% in the lower Mariño and Río de los Pozos Formations, to almost completely swamping the zircon signature in the Tobas Angostura Formation (85%; Fig. 11).

STRATIGRAPHIC AGE CONSTRAINTS

The absolute age of Cacheuta basin strata is constrained by U-Pb geochronology on volcanic tuff samples, the MDA of the youngest U-Pb detrital zircon subpopulation (this work), and by $^{40}Ar/^{39}Ar$ ages on volcanic tuff biotite and hornblende and magnetostratigraphy from Irigoyen et al. (2000).

Detrital zircon analyses from throughout the Cacheuta basin yield an abundance of young Cenozoic grains (Fig. 12). Normalized age probability plots of the youngest U-Pb detrital zircon subpopulation within stratigraphically arranged detrital and volcanic tuff samples define a distinct younging array from the base of the Mariño Formation to the top of Río de los Pozos Formation (Fig. 12). The gradational younging upward patterns of the youngest U-Pb zircon subpopulations, coupled with the direct overlap between these age peaks and U-Pb zircon ages and $^{40}Ar/^{39}Ar$ biotite and hornblende ages from intercalated volcanic tuff, support our interpretation that the MDA accurately reflects the true depositional age of the samples (Table 2).

Geochronology of Cacheuta basin strata record at least ~12 m.y. (ca. 20 Ma to younger than 7.5 Ma) of basin evolution (Fig. 4). The timing of initial basin subsidence is constrained by the lowermost sample in the Mariño Formation, which yields an MDA of 19.2 ± 0.26 Ma (Table 2). This sample was collected ~75 m above the contact with the underlying Divisadero Largo Formation (Fig. 4), and the age of initial basin

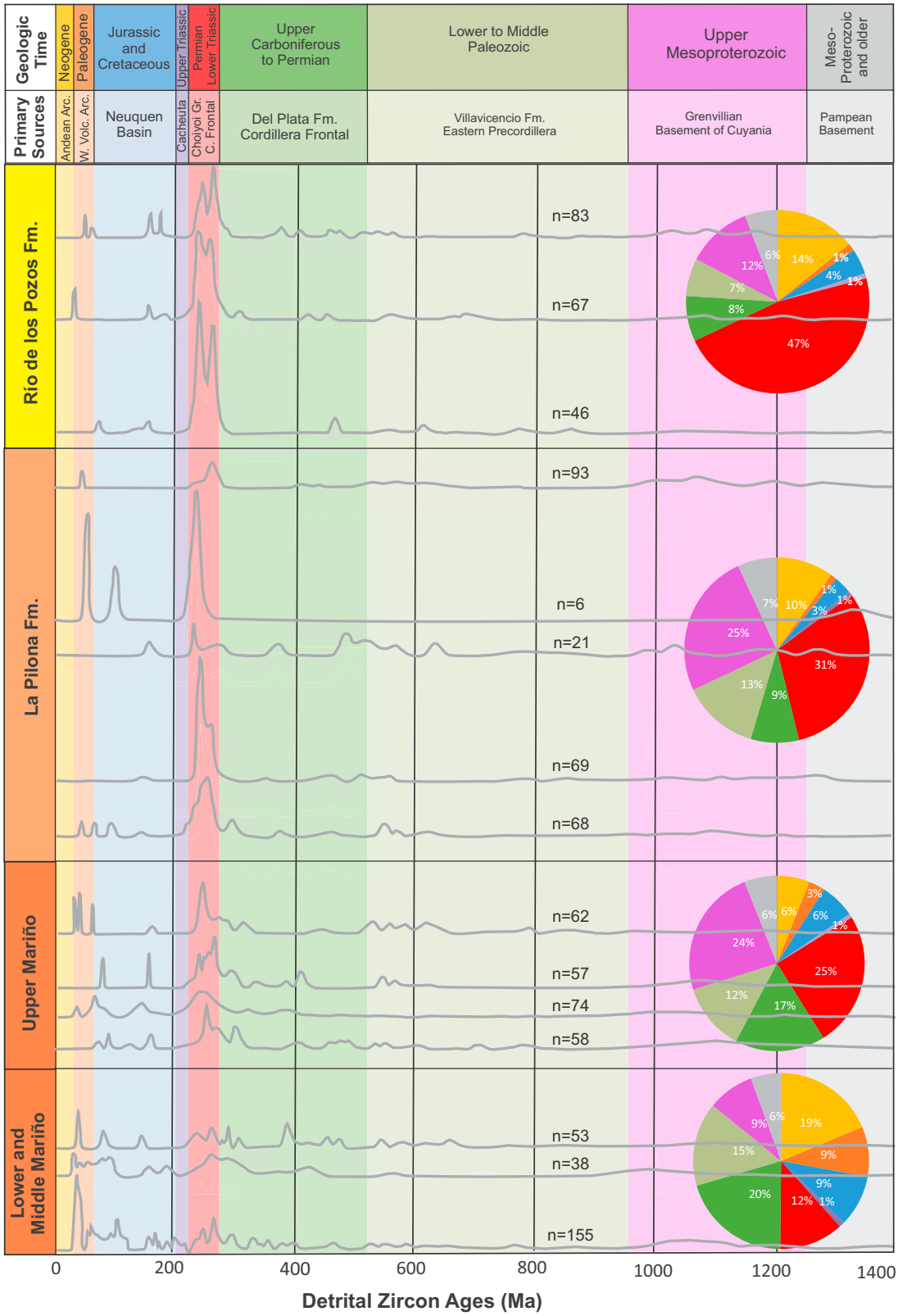

Figure 11. Comparative plot of normalized detrital zircon U/Pb age distributions for Cacheuta basin strata arranged in stratigraphic order. Color bars correspond to probable source regions in the south-central Andes. Pie diagrams display U/Pb detrital data binned according to age and source area to display stratigraphic trends in provenance. Pie diagram colors correspond to the color of the age range of the probable source area as illustrated in the upper banner. C.—Cordillera; Fm—Formation; Gr—Group.

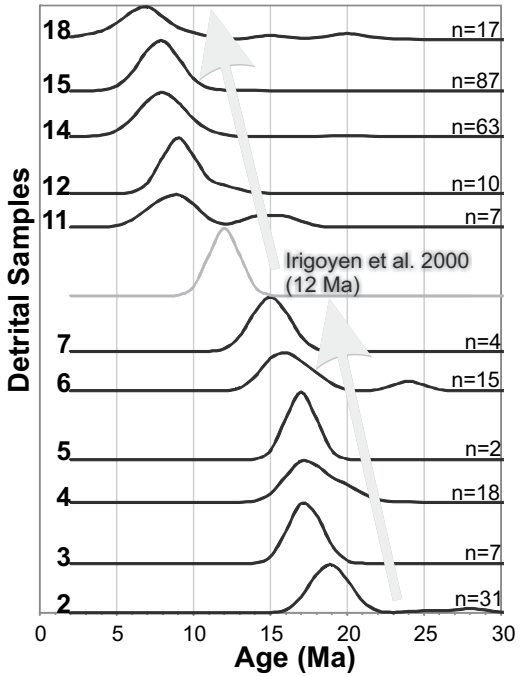

Figure 12. Normal probability plot of Cenozoic U/Pb ages displayed in stratigraphic order from the base of the Mariño Formation to the highest sample located in the middle of Río de los Pozos Formation (*n*—number of Cenozoic zircons in the peak). Stratigraphically stacked Cenozoic ages depict a distinct decrease in age up section, supporting the interpretation that maximum depositional ages reflect true depositional age of facies.

subsidence is interpreted to be ca. 20 Ma, which is ~4 m.y. older than previous interpretations (Irigoyen et al., 2000; Cerdeño, 2007).

The estimated 20 Ma age of initial subsidence is based on our reinterpretation of the Cacheuta magnetostratigraphy coupled with new detrital ages. The magnetic polarity stratigraphy of Cenozoic strata in the Cacheuta area was determined by Irigoyen et al. (2000) and correlated tentatively with the geomagnetic polarity time scale (GPTS) of Baksi (1993) aided by $^{40}Ar/^{39}Ar$ dates mostly from the La Pilona Formation. However, new zircon U-Pb dates demonstrate that the base of the Mariño Formation is several million years older than indicated by Irigoyen et al. (2000), thus requiring reinterpretation of the magnetic polarity correlations. The key section is the ~800-m-thick Tosca de Mariño section, which includes 36 sites in the Mariño Formation (Irigoyen et al., 2000) that record at least 15 geomagnetic reversals over 772 m of section. The lower part of the Mariño section is notable for a long dominantly normal polarity interval that encompasses the prominent eolian sandstone beds near the base of the section, although, as noted by Irigoyen et al. (2000), this might reflect a normal viscous overprint that was not removed by thermal demagnetization of the samples rather than a primary polarity. Above this, there are series of short polarity intervals that are based in most cases on data from single sites. Irigoyen et al. (2000) matched this Mariño sequence of reversals to the Baksi (1993) GPTS between 15.8 and ca. 12.0 Ma, with the dominantly long normal interval near the base of the section corresponding to C5ADn-C5ACn. However, new U-Pb geochronology demonstrates that this same sequence of Mariño reversals is correlative to the Gradstein et al. (2004) GPTS between 20.1 and 13.7 Ma, with the long normal interval at the base of the section corresponding to C6n-C5En. Although firm correlation of specific polarity zones is difficult to achieve (cf. Irigoyen et al., 2000), the series of short polarity zones above this corresponds well to the series of short polarity intervals above C5En (Fig. 13).

Syndepositional zircon is sparse at the Mariño–La Pilona contact; three samples within ~100 m of the contact yielded only six Miocene zircon grains (Fig. 4; Table DR4 [see footnote 1]). One sample (MA-5) ~100 m above the contact yielded an unsatisfactory MDA of 15.4 ± 1.9 Ma (n = 2), which must be viewed with caution. The age of the upper Mariño–La Pilona contact is therefore interpreted to be 12.03 ± 0.45 Ma, based on a $^{40}Ar/^{39}Ar$ hornblende age from Irigoyen et al. (2000).

Irigoyen et al. (2000) correlated a faulted section of Mariño Formation strata beneath La Pilona Formation in their Arroyo del Agua Blanca section (section II in this work) to the GPTS C5An normal interval, equivalent to the upper part of Mariño Formation strata in the Tosca de Mariño section. However, we found no evidence of fault repetition in this section of the Mariño Formation. Honoring the 12.03 ± 0.45 Ma hornblende $^{40}Ar/^{39}Ar$ date reported by Irigoyen et al. (2000) from an ash-fall bed in this section, we instead correlate these strata to C5AAn-CrAn in the Gradstein et al. (2004) GPTS, which requires these strata to be younger than Mariño beds at the top of the Tosca de Mariño section. The Irigoyen et al. (2000) GPTS correlation of the La Pilona Formation is consistent with the new data. Our revised magnetic polarity correlations are consistent with an unconformity of ~1 m.y. duration between the Mariño and La Pilona Formations, as originally proposed by Irigoyen et al. (2000); however, we cannot confidently eliminate the possibility of a continuous succession between these two units.

Approximately 1180 m of sediment were deposited during the ~7.2 m.y. of Mariño Formation deposition, suggesting a sedimentation rate (compacted) of ~0.16 mm/yr (Fig. 14). This sedimentation rate is lower than the 0.22 mm/yr previously calculated by Irigoyen et al. (2000), due to new geochronologic data that indicate basin subsidence began at ca. 20 Ma.

TABLE 2. CACHEUTA U/Pb ZIRCON AGES

ID	Name	Latitude (°S)	Longitude (°W)	Formation	Age (Ma)	Age type
18	134JBM11	33.1441	69.0743	Rio de los Pozos	7.41 ± 1.3	MDA
15	132JBM14	33.1317	69.1734	Tobas La Angostura	8.39 ± 0.42	Tuff
14	133JBM14	33.1501	69.0850	Tobas La Angostura	8.31 ± 0.48	Tuff
12	114JBM13	33.1043	69.2187	La Pilona	9.6 ± 1.1	Tuff
11	113JBM13	33.0935	69.2002	La Pilona	9.47 ± 0.89	Tuff
7	03_MA	32.9781	69.1812	Mariño	15.6 ± 1.0	MDA
6	111JBM13	33.0537	69.1873	Mariño	16.3 ± 0.83	MDA
5	02_MA	32.9869	69.1762	Mariño	17.4 ± 1.3	MDA
4	01_MA	32.9903	69.1669	Mariño	17.58 ± 0.28	MDA
3	108JBM13	33.0512	69.1753	Mariño	17.96 ± 0.2	Tuff
2	106JBM13	33.0472	69.1757	Mariño	19.2 ± 0.26	MDA

Note: MDA—Maximum Depositional Age.

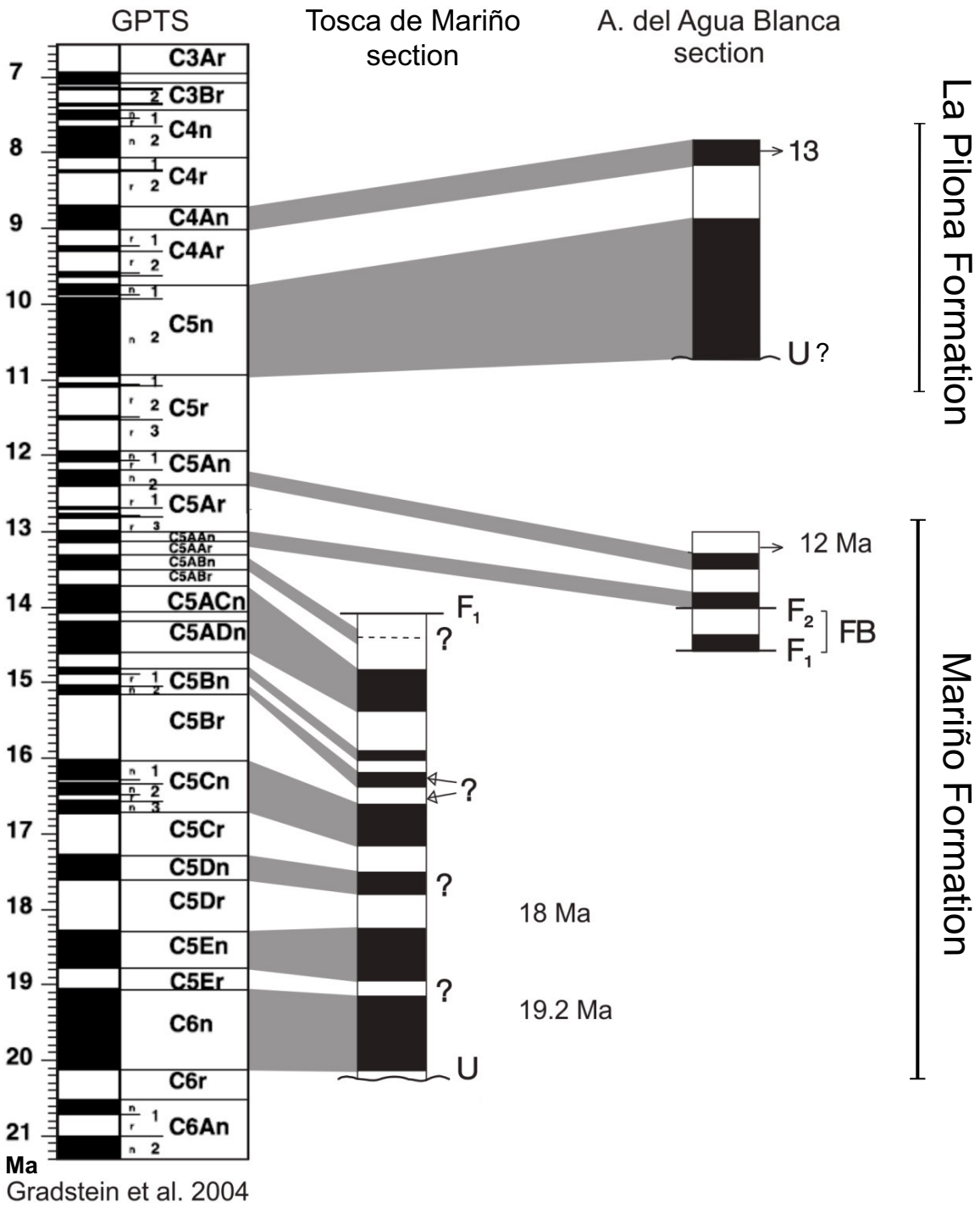

Figure 13. Reinterpretation of magnetic data collected by Irigoyen et al. (2000), following geomagnetic polarity time scale (GPTS) of Gradstein et al. (2004). Black zones represent normal polarity; white zones represent reversed polarity. F1 and F2 are faults discussed by Irigoyen et al. (2000) that are not supported by detailed field work. The fault-bounded block in the Arroyo del Agua Blanca section (FB) is interpreted to be in normal stratigraphic continuity within the normal magnetic interval corresponding to chron C5ABn. U—unconformity.

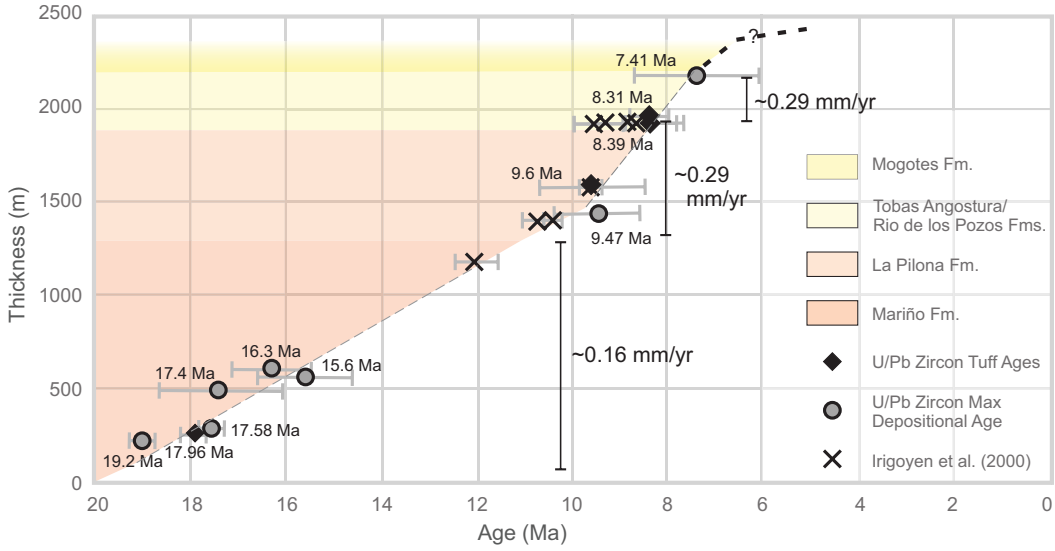

Figure 14. Cacheuta basin subsidence curve. Ages are constrained by U/Pb zircon maximum depositional ages (gray circles), ^{40}Ar-^{39}Ar biotite and hornblende ages from Irigoyen et al. (2000; X-symbol), and U/Pb tuff ages (black diamonds).

The upper boundary of the La Pilona Formation is constrained by an 8.39 ± 0.42 Ma U-Pb zircon age on volcanic tuff from the base of the overlying Tobas Angostura Formation (Fig. 4; Table 2), which overlaps with a 9.30 ± 0.68 Ma $^{40}Ar/^{39}Ar$ hornblende age (Irigoyen et al., 2000) from a similar stratigraphic level. The La Pilona Formation accumulated approximately ~860 m of coarse clastic sediment in ~3 m.y, suggesting a sedimentation rate (compacted) of 0.28 mm/yr, i.e., nearly double that of the underlying Mariño Formation (Fig. 14). This significant increase in sedimentation rate is interpreted to represent increased orogenic exhumation due to eastward migration of the deformation front that produced a shift in sedimentation from distal to proximal foredeep facies.

The base of the tuffaceous facies of the Tobas Angostura Formation is well constrained by U-Pb zircon ages in volcanic tuff to span an age from ca. 8.31 to 8.39 Ma (Fig. 4; Table 2). The upper contact of the Tobas Angostura is constrained by a 7.41 ± 0.66 Ma U-Pb zircon MDA from a sample near the base of the overlying Río de los Pozos Formation. The Tobas Angostura Formation accumulated ~160 m of tuffaceous sediment in ~1 m.y., indicating a sedimentation rate of ~0.16 mm/yr, consistent with a hiatus in structural deformation concomitant with a late Miocene volcanic event.

The Río de los Pozos Formation represents a return to coarse clastic sedimentation in the Cacheuta basin. Syndepositional zircon is sparse, with only one of three samples in the formation yielding a robust young population that constrains the MDA of the middle of the formation to be 7.41 ± 1.3 Ma (Fig. 4; Table 2). Limited outcrop exposure of the overlying Mogotes Formation prevented application of detrital zircon geochronology to the unit, which can only be constrained as younger than ca. 7.4 Ma, but which is potentially significantly younger.

DISCUSSION

Sediment Sources

Integration of stratigraphic and sedimentologic trends with provenance data suggests tight linkages between orogenesis and basin evolution. The Cacheuta basin contains several conspicuous coarse clastic pulses and distinct shifts in provenance that may be utilized to constrain the timing of deformational events and track the migration of the orogenic front and retroarc foreland basin through time.

Most notable throughout the point count, conglomerate clast count, and U-Pb detrital age trends is the dominance of detritus derived from the Permian–Triassic Choiyoi Group of the Cordillera Frontal (Sato et al., 2015; Rocha-Campos et al., 2011; Spalletti et al., 2009; Kay et al., 1989; Cingolani et al., 2012). The presence of Choiyoi Group detritus in the base of the Mariño Formation is critical, as it requires that the Choiyoi Group has been exposed as a sediment source since at least the early Miocene (Hoke et al., 2015). Provenance data from older strata, including the Paleogene Divisadero Largo Formation (Mahoney et al., 2016) and Jurassic to Cretaceous strata of the Neuquen Basin (Naipauer et al., 2015; Horton et al., 2016; Balgord, 2017), require that the Choiyoi Group has been a consistent sediment source since at least the Early Jurassic. This observation is at odds with the traditional interpretation of the development of the Aconcagua fold-and-thrust belt and retroarc foreland basin, which proposes a steady west-to-east migration of structural deformation, with uplift of the Cordillera Frontal at ca. 9 Ma (Giambiagi et al., 2001; Ramos et al., 2002). Both detrital zircon data and conglomerate clast count data require that at least some part of the Cordillera Frontal has been a positive topographic element throughout the evolution of the Cacheuta basin, with sediment supply from the Choiyoi Group episodically enhanced during thrust belt propagation.

Stratigraphic and sedimentologic variations suggest that the Cacheuta basin strata record several distinct deformational events during the evolution of the basin. Integration of these variations with provenance trends derived from clast counts and U-Pb detrital zircon ages constrains the sequential migration of the Aconcagua fold-and-thrust belt, as well as deformational events in the Cordillera Frontal and the Precordillera.

The lower and middle parts of the Mariño Formation contain the most heterogeneous assemblage of detrital zircon within the Cacheuta basin. The lowermost sample of Mariño Formation strata analyzed contains a large proportion of Eocene and Oligocene zircon (56–26 Ma) that are only weakly represented higher in the basin stratigraphy. This distinct signal may reflect unroofing of poorly known Paleogene volcanic rocks on the western side of the Andes in Chile or, alternatively, reworking of subjacent Paleogene strata (e.g., Divisadero Largo Formation—Mescua et al., 2017; Chocolate Arenites of the Manantiales basin—Mazzitelli et al., 2015; Puesto la Flecha Formation—Fosdick et al. 2017), which contain a large component of Eocene–Oligocene zircon. Paleocene detrital zircon (9%) within the lower Mariño Formation matches the age of zircon within

the underlying Paleocene Divisadero Largo Formation and may have been derived by erosion of subjacent strata, perhaps due to eastward migration of the forebulge early in the evolution of the basin. Jurassic and Cretaceous zircon (9%) in the Cacheuta basin is likely derived from Mesozoic strata of the Neuquén Basin uplifted within the Aconcagua fold-and-thrust belt of the Cordillera Principal (Fig. 15; Giambiagi et al., 2001; Ramos et al., 2002; Ramos and Folguera, 2009; Balgord, 2017). This interpretation is supported by conglomerate clasts, including red sandstone from the Upper Jurassic Tordillo Formation and limestone from Lower Cretaceous carbonates of the Mendoza Group, which are most likely derived from the successions exposed within the Aconcagua fold-and-thrust belt (Figs. 2, 11, and 15; Giambiagi et al., 2009). Orogenic exhumation of the Cordillera Principal in early Miocene time (ca. 20 Ma) is also suggested by the presence of andesite clasts derived from Andean volcanism and by the abundance of Miocene zircon (19%), potentially derived from shallow subduction-related plutons in the Cordillera Principal (Kay et al., 2005). It is important to note that the presence of Permian–Triassic detrital zircon (12%) as well as the significant population of Choiyoi Group clasts in conglomerates and sandstones require that some parts of Cordillera Frontal had enough structural relief to supply sediment to the Cacheuta basin between ca. 20 and 17 Ma but did not inhibit sediment transport from the Cordillera Principal. This paleogeographic configuration may have been the result of uplift of a portion of the Cordillera Frontal to the north, in the Cordón del Espinacito (Alarcón and Pinto, 2015) or Cordillera del Tigre (Fig. 15). This configuration is consistent with paleocurrent data and with the occurrence of fine-grained Choiyoi Group detritus in the Tunuyán basin to the south, which requires a distal source (Porras et al., 2016).

A significant provenance shift occurs at the boundary between the middle and upper Mariño Formation (ca. 16.3 Ma), marked by a change in detrital zircon population, sandstone petrography, conglomerate clast composition, and depositional environment, and by a significant increase in clast size. There is a distinct increase in Permian–Triassic zircon (12% to 25%), derived from the Choiyoi Group, and Mesoproterozoic (9% to 24%) zircon, derived from Paleozoic sedimentary strata within the Cordillera Frontal (Fig. 11). This provenance shift is interpreted to represent eastward migration of the thrust front into the Cordillera Frontal at this latitude, which resulted in structural uplift of the Cordon del Plata block of the Cordillera Frontal, and probably the western Precordillera (Fig. 15). Eastward migration of the focus of deformation resulted in progradation of proximal facies into the retroarc foreland basin. This migration led to a decrease in sediment supply from the Cordillera Principal, marked by a steady decrease in andesite, limestone and red sandstone conglomerate clasts derived from the Cordillera Principal, concomitant with an increase in rhyolite and metasandstone clasts from the Cordillera Frontal (Figs. 11 and 15). The distinct spike in andesite, limestone, and red sandstone clasts at the boundary between the middle and upper Mariño Formations may represent cannibalization of Neogene piggyback basin strata during migration of the thrust front (Fig. 9). The eastward shift of the deformation front is also supported by sandstone provenance analysis, which records a distinct decrease in andesitic volcanic detritus derived from the Cordillera Principal, and an increase in rhyolitic volcanic detritus derived from the Choiyoi Group of the Cordillera Frontal (Figs. 9 and 10).

Renewed episodic eastward migration of deformation is indicated by a second major shift in grain size, clast composition, and detrital zircon population at the Mariño–La Pilona contact (ca. 11 Ma). There is a distinct change in sediment composition and depositional environment at the Mariño–La Pilona transition, with the development of disorganized, channelized cobble to boulder conglomerate (FA5), which marks the continued migration of proximal facies eastward (Figs. 4 and 15). The most distinct compositional shift is the marked increase in green siltstone/sandstone, reflecting uplift of the Devonian Villavicencio Group of the eastern Precordillera (Fig. 9). The detrital zircon spectra are also dominated by Permian–Triassic zircon derived from the Choiyoi Group of the Cordillera Frontal and Mesoproterozoic and Paleozoic zircon derived from the western Precordillera (Fig. 11). The La Pilona Formation is dominated by proximal detritus derived from the Cordillera Frontal and Precordillera, constraining the position of the leading edge of the thrust front between ca. 11 and 8 Ma, consistent with the timing of uplift for the Precordillera estimated by Walcek and Hoke (2012).

The Tobas Angostura Formation is dominated by first-cycle pyroclastic and reworked pyroclastic debris, and it lacks coarse clastic detritus. This suggests a hiatus in the eastward migration of deformation between ca. 8.4 and 7.4 Ma, concomitant with a major volcanic event.

Volcanogenic sedimentation of the Tobas Angostura Formation is superseded by clastic sedimentation represented by the Río de los Pozos Formation. The age of the Tobas Angostura–Río del los Pozos Formation contact is poorly constrained but is assumed to be ca. 7.4 Ma. The Río de los Pozos Formation is distinctly finer grained than the La Pilona Formation, and it is dominated by detrital zircon derived from the Choiyoi Group (47%; Fig. 10). Miocene detrital zircon is also significant (12%) and was probably derived from reworking of the subjacent Tobas Angostura Formation or supplied by waning stage volcanism. It is unclear if the return of clastic sedimentation evident in the Río del los Pozos Formation represents renewed uplift of the orogenic belt, or simply ongoing erosion of the orogeny following cessation of volcanic activity.

The most recent structural event in the Cacheuta basin is indicated by a major change in grain size, sedimentary facies, and provenance at the base of the Mogotes Formation (ca. 7.4 Ma). The Mogotes Formation is poorly exposed and loosely consolidated with an unknown maximum thickness. The Mogotes Formation has a sharp contact with the underlying Río de los Pozos Formation and is characterized by disorganized boulder conglomerate dominated by rhyolite clasts. The distinct change in grain size and highly disorganized fabric suggest that the Mogotes Formation represents rapid sedimentation in a proximal alluvial-fan setting, probably immediately adjacent to active thrust faults within the Cordillera Frontal.

Andean Foreland System Evolution

The classic model of the Miocene evolution of the Andean system involves progressive eastward migration of the Aconcagua orogenic wedge, beginning with uplift of the Cordillera Principal at ca. 18 Ma, followed by successive uplift of the Cordillera Frontal and then the Precordillera (Ramos et al., 1996, 2002). Structural deformation was episodic, with a major contractional phase in the middle Miocene, a quiescent period in the middle to late Miocene, and out-of-sequence thrust reactivation and thick-skinned fold-and-thrust belt deformation in the Cordillera Frontal starting in the late Miocene (ca. 9 Ma; Irigoyen et al., 2000) Eastward migration of the orogenic wedge resulted in loading of the retroarc foreland basin and formation of wedge-top, foredeep, forebulge, and back-bulge depozones throughout the Miocene. Our detailed stratigraphic, sedimentologic, and geochronologic analysis of the Cacheuta basin requires revision of this model.

Initial subsidence of the Cacheuta basin was driven by tectonic shortening in the Cordillera Principal at ca. 20 Ma and the uplift of the Espinacito range (Cordillera Frontal) north of 32.5°S (Alarcón and Pinto, 2015). The western side of the Cacheuta basin was apparently largely removed by cannibalization of piggyback basins during migration of the thrust belt.

The Mariño Formation unconformably overlies the Paleogene Divisadero Largo Formation (ca. 50 Ma), suggesting an ~30 m.y. period of erosion or nondeposition. The disconformable contact is bedding parallel and marked by a thin (30 cm) pebble to cobble conglomerate bed with little

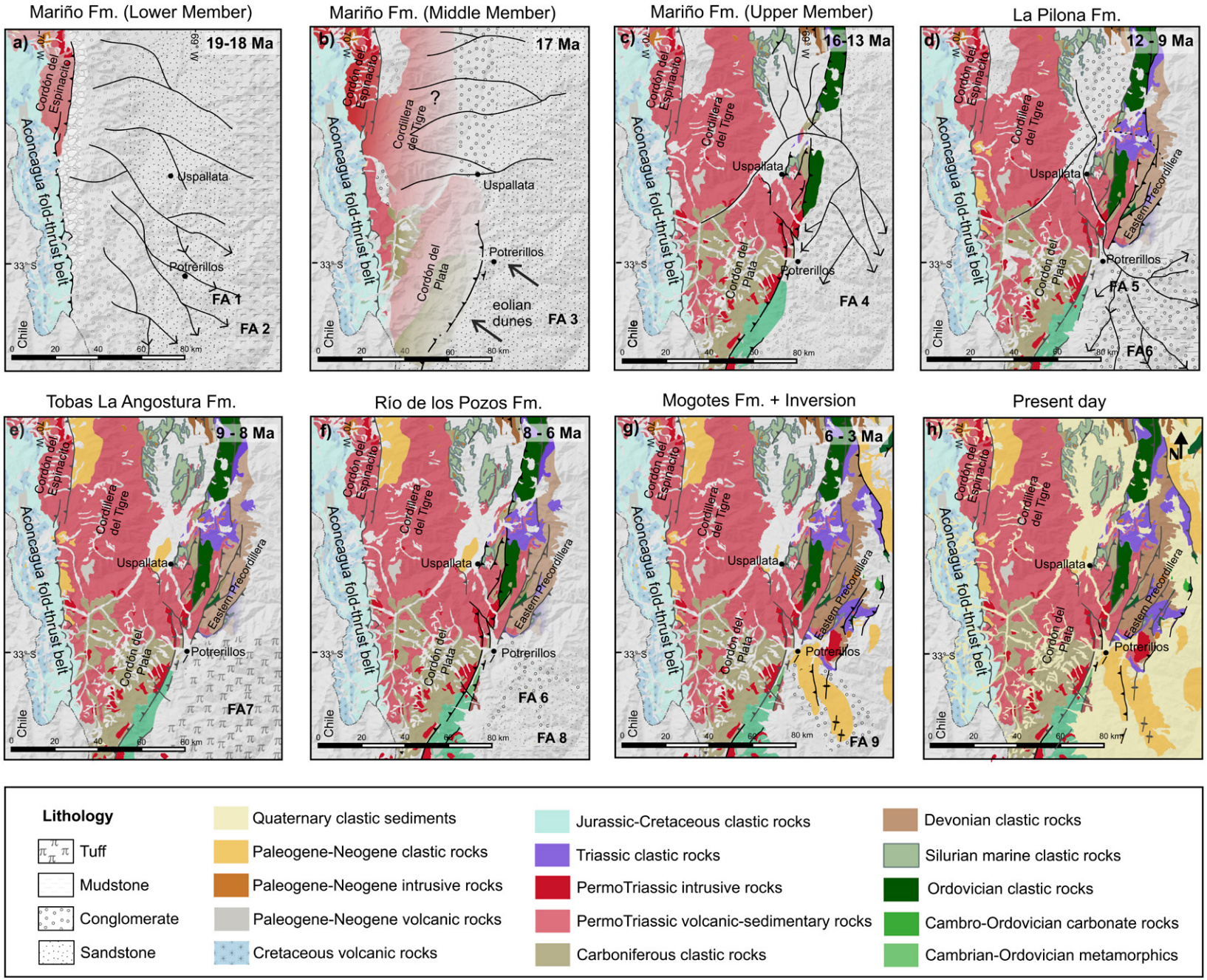

Figure 15. Paleogeographic reconstruction of the Cacheuta retroarc foreland basin from early Miocene to present, schematically illustrating the spatial and temporal evolution of the depocenter. The distribution of geologic units exposed during each time slice was inferred from the integration of detrital zircon, conglomerate clast count, and petrographic data, coupled with structural data from companion studies (e.g., Giambiagi et al., 2012; Hoke et al., 2014).

evidence of significant erosional beveling. The occurrence of Paleocene detrital zircon in the Mariño Formation is consistent with migration of the retroarc forebulge and cannibalization of subjacent strata during eastward migration of the orogenic wedge during the early Miocene (e.g., Horton et al., 2001; DeCelles and Horton, 2003; DeCelles et al., 2011). Alternatively, the occurrence of a similar Eocene–earliest Miocene stratigraphic hiatus to the south (Atuel basin; Horton et al., 2016) and to the north (Manantiales basin; Mahoney et al., 2016) suggests a regional period of nondeposition that may represent a period of tectonic quiescence coupled with limited flexural rebound following cessation of Late Cretaceous thrust loading (Horton et al., 2016; Balgord, 2017).

Detrital zircon provenance data and conglomerate composition require that the Choiyoi Group of the Cordillera Frontal was exposed and providing detritus in the earliest stages of basin evolution. The occurrence of Choiyoi-derived zircon in both Paleogene (Mahoney et al., 2016) and Jurassic to Cretaceous (Balgord, 2017) sedimentary units requires that the Choiyoi Group has been at the surface supplying sediment since at least Jurassic time. This is supported by thermochronologic data (Fosdick et al., 2017; Lossada et al., 2017), which suggests that portions of the Cordillera Frontal north of the study area (30°S) have been topographic highs since Eocene time. While eastward migration of deformation in Miocene time may have renewed uplift of the Cordillera Frontal, it was not responsible for initial uplift of the Cordillera Frontal.

The preserved sedimentary record in the Cacheuta basin records initial subsidence in a distal retroarc foredeep (ca. 20–18 Ma) characterized by low-energy braided streams with laterally stable areas accumulating paleosols and ephemeral lake deposits. At this time, the magmatic arc was located in the western slope of the Cordillera Principal, and the Aconcagua fold-and-thrust belt began to develop in a trans-arc position (Ramos et al., 1996). Initial sedimentation in the Mariño Formation reflects an arid ephemeral fluvial environment at ca. 20 and 19 Ma (Fig. 15A), during the development of high-standing topography in the Cordillera Principal. The depositional setting transitioned to an eolian environment between 18 and 17 Ma (Fig. 15B), perhaps due a rain shadow effect. By ca. 17 Ma, the Cacheuta basin registered the onset of uplift of the Cordón del Plata range (Fig. 15C). This eastward migration of the orogenic wedge led to a drainage reorganization and the development of fluvial megafans with complexly interfingering braided stream channels, sandy lobes, and muddy interchannel zones that represent the majority of sediments within the depocenter (Fig. 15C).

The transition between the middle and upper Mariño Formation (ca. 16.3 Ma) marks the initial progradation of proximal foredeep deposits into the Cacheuta basin, driven by ongoing uplift of the Cordón del Plata range and its northward migration into the western sector of the Precordillera (Fig. 15C). By this time (ca. 15.6 Ma; Ramos et al., 1996), the magmatic arc had migrated from the western slope of the Cordillera Principal to the eastern slope, and it localized at the Aconcagua volcanic complex. Episodic deformation within the orogenic wedge controlled the rate of basin subsidence throughout its history.

The Mariño–La Pilona contact (ca. 11 Ma) marks the initiation of major subsidence in the basin from 11 to 8.6 Ma, as evidenced by the progradation of a megafan system into the proximal foredeep and migration of distal facies to the east (Fig. 15). The dramatic increase in green lithic arenite derived from the Devonian Villavicencio Formation in the La Pilona Formation requires incorporation of the eastern Precordillera into the thrust system by this time (Fig. 15D). The major increase in sedimentation at the Mariño–La Pilona contact is thought to reflect (1) the climax in thrusting along the La Carrera fault system, which uplifted the Cordón del Plata range and significantly increased the orogenic load, and (2) the involvement of the eastern Precordillera into the orogenic wedge.

Contractional shortening in the Andes at 33°S slowed at ca. 8.6 Ma, coeval with major pyroclastic and resedimented pyroclastic sedimentation in the Tobas Angostura Formation (Figs. 4 and 15E) and the waning stage of volcanism in the Aconcagua complex. The cessation of volcanism may have been coeval with renewed motion of the La Carrera fault system, which would have led to a rejuvenation of proximal foredeep sedimentation represented by the Río de los Pozos Formation (Fig. 15F) and an increase in detritus from the Cordillera Frontal. Continued eastward migration of the orogenic system culminated in the deposition of the coarse disorganized cobble-boulder conglomerates of the Mogotes Formation, which represent either proximal foredeep or wedge-top deposits within the retroarc foreland basin (Figs. 15G and 15H; DeCelles and Giles, 1996).

Tectonic Implications

The results of this investigation require reevaluation of the role of flat-slab subduction in relation to orogenic exhumation. Slab shallowing in the south-central Andes began at ca. 12 Ma, coincident with the arrival of the Juan Fernández Ridge to the trench at 33°S (Yáñez et al., 2001; Ramos et al., 2002). Previous works interpreted the onset of eastward migration of deformation, including the uplift of the Cordillera Frontal, to have taken place at ca. 9 Ma, as a response to slab shallowing. In contrast, our results indicate that the Cordillera Frontal was a primary sediment source to the Cacheuta basin since at least the beginning of deposition of the Mariño Formation at 20 Ma. Distinct shifts in sedimentation patterns and provenance, including a major influx of detritus from the Precordillera, indicate that a significant increase in subsidence occurred in the Cacheuta basin between ca. 11 and 8.6 Ma. This major shift in basin dynamics associated with uplift of the Precordillera could have been related to initiation of flat-slab subduction in the region. However, recent work has demonstrated major shifts in provenance, dramatically increased shortening and widespread thrust displacement in the early late Miocene in the southern, central, and northern Precordillera (Levina et al., 2014; Fosdick et al., 2015; Suriano et al., 2017). This essentially simultaneous deformation in the Precordillera between ca. 12 and 9 Ma along >350 km of strike length (~30°S–33°S) conflicts with the proposed progressive southern migration of flat-slab subduction (Kay and Mpodozis, 2002; Yáñez et al., 2001; Ramos et al., 2002). While there is evidence for a north-to-south migration of deformation along the orogenic front of the Cordillera Frontal, this migration occurred between ca. 20 and 17 Ma, ~5–8 m.y. prior to the proposed initiation of flat-slab subduction in the region. These timing constraints suggest the Cordillera Principal, Cordillera Frontal, and Precordillera seem to have been uplifted during normal subduction-related orogenic processes prior to the initiation of flat-slab subduction in the area. It is feasible that the initiation of flat-slab subduction contributed to the early late Miocene contractional deformation; however, it is apparent that the primary effect of flat-slab subduction on upper-crustal deformation was the development of the broken foreland and uplift of the Sierras Pampeanas. Orogenic exhumation in the south-central Andes appears to be controlled instead by upper-crustal architecture influenced by inherited structural and stratigraphic elements (e.g., Kley et al., 1999).

CONCLUSIONS

The results presented herein allow us to reevaluate the role of flat-slab subduction in relation to orogenic exhumation. Our results indicate that the Cordillera Frontal was in part a topographic high since at least the beginning of deposition of the Mariño Formation at 20 Ma, particularly along the Espinacito Range, north of 32.5°S. In addition, renewed uplift of the Cordillera Frontal and initiation of uplift in the Precordillera at

14–13 Ma occurred much earlier than previously inferred and could not have been related to the inception of slab shallowing (Levina et al., 2014; Suriano et al., 2017).

These results suggest that uplift of the Cordillera Principal, Cordillera Frontal, and Precordillera, and concomitant development of the Cacheuta retroarc foreland basin, in the early to mid-Miocene was the result of contractional deformation and crustal thickening during normal subduction-related orogenic processes. The primary upper-crustal response to the development of the flat slab in late Miocene time was development of the broken foreland of the Sierras Pampeanas (Ramos et al., 2002) and exhumation of older strata of the Cacheuta basin (Buelow et al., 2014; Buelow, 2015).

ACKNOWLEDGMENTS

Victor Ramos provided inspiration and samples from the Potrerillos section. We would like to thank the Hostel Alamo and Las Carditas for their hospitality. We appreciate the efforts of several University of Wisconsin–Eau Claire (UWEC) alumni and undergraduate students for initial work in the Cacheuta basin and for their help in the sample preparation process. Special thanks go to the University of Arizona LaserChron Center for geochronologic expertise. This project was supported by the National Science Foundation (NSF award number 12–50402) to San Diego State University and UWEC, UWEC International Fellows, the UWEC Blugold Commitment program, and the Agencia Nacional de Promoción Científica y Tecnológica (PICT 2011–1079). Reviews by Brian Horton and an anonymous reviewer significantly enhanced the manuscript.

REFERENCES CITED

Alarcón, P., and Pinto, L., 2015, Neogene erosion of the Andean Cordillera in the flat-slab segment as indicated by petrography and whole-rock geochemistry from the Manantiales Foreland Basin (32°–32°30′S): Tectonophysics, v. 639, p. 1–22, https://doi.org/10.1016/j.tecto.2014.11.001.

Allmendinger, R.W., and Judge, P.A., 2014, The Argentine Precordillera: A foreland thrust belt proximal to the subducted plate: Geosphere, v. 10, p.1203–1218, https://doi.org/10.1130/GES01062.1.

Astini, R.A., Dávila, F.M., López Gamundí, O., Gómez, F., Collo, G., Ezpeleta, M., Martina, F., and Ortiz, A., 2005, Cuencas de la región precordillerana, *in* Chebli, G., Cortiñas, J., Spalletti, L., Lagarreta, L., and Vallejo, E., eds., Frontera Exploratoria de la Argentina: VI Congreso de Exploracion y Desarrollo de Hidrocarburos, Ampliando las Fronteras: Mar del Plata, Argentina, IAPG (Instituto Argentino del Petróleo y del gas), p. 115–141.

Baksi, A.K., 1993, A geomagnetic polarity time scale for the period 0–17 Ma, based on $^{40}Ar/^{39}Ar$ plateau ages for selected field reversals: Geophysical Research Letters, v. 20, p. 1607–1610, https://doi.org/10.1029/93GL01876.

Baldis, B., Beresi, M., Bordonaro, O., and Vaca, A., 1984, The Argentine Precordillera as a key to Andean structure: Episodes, v. 7, p. 14–19.

Balgord, E.A., 2017, Triassic to Neogene evolution of the south-central Andean arc determined by detrital zircon U-Pb and Hf analysis of Neuquén Basin strata, central Argentina (34°S–40°S): Lithosphere, v. 9, p. 453–462 https://doi.org/10.1130/L546.1.

Barazangi, M., and Isacks, B.L., 1976, Spatial distribution of earthquakes and subduction of the Nazca plate beneath South America: Geology, v. 4, no. 11, p. 686–692, https://doi.org/10.1130/0091-7613(1976)4<686:SDOEAS>2.0.CO;2.

Beratan, K.K., Hsieh, J., and Murray, B., 1999, Pliocene–Pleistocene stratigraphy and depositional environments, southern Confidence Hills, Death Valley, California, *in* Wright, L.A., and Troxel, B., eds., Cenozoic Basins of the Death Valley Region: Geological Society of America Special Paper 333, p. 289–300, https://doi.org/10.1130/0-8137-2333-7.289.

Blikra, L.H., and Nemec, W., 1998, Postglacial colluvium in western Norway: Depositional processes, facies and palaeoclimatic record: Sedimentology, v. 45, no. 5, p. 909–959, https://doi.org/10.1046/j.1365-3091.1998.00200.x.

Bull, W.B., 1997, Discontinuous ephemeral streams: Geomorphology, v. 19, p. 227–276, https://doi.org/10.1016/S0169-555X(97)00016-0.

Cahill, T., and Isacks, B.L., 1992, Seismicity and shape of the subducted Nazca plate: Journal of Geophysical Research, v. 97, p. 17503, https://doi.org/10.1029/92JB00493.

Capaldi, T.N., Horton, B.K., McKenzie, N.R., Stockli, D.F., and Odlum, M.L., 2017, Sediment provenance in contractional orogens: The detrital zircon record from modern rivers in the Andean fold-thrust belt and foreland basin of western Argentina: Earth and Planetary Science Letters, v. 479, p. 83–97.

Cerdeño, E., 2007, Systematic position of the Mesotheriidae (Notoungulata) from the Mariño Formation (Miocene) in Divisadero Largo, Mendoza, Argentina: Geobios, v. 40, no. 6, p. 767–773, https://doi.org/10.1016/j.geobios.2007.01.003.

Charrier, R., Pinto, L., and Rodríguez, M.P., 2007, Tectonostratigraphic evolution of the Andean orogen in Chile, *in* Moreno, T., and Gibbons, W., eds., The Geology of Chile: Geological Society, London, p. 21–114.

Cingolani, C.A., Uriz, N., Chemale, F., Jr., and Varela, R., 2012, Las rocas monzoníticas del sector oriental del plutón de Cacheuta, Precordillera mendocina: Características geoquímicas y edad U-Pb (LA-ICP-MS): Revista de la Asociación Geológica Argentina, v. 69, no. 2, p. 195–206.

Damanti, J.F., 1993, Geomorphic and structural controls on facies patterns and sediment composition in a modern foreland basin, *in* Marzo, M., and Puigdefábregas, C., eds., Alluvial Sedimentation: International Association of Sedimentologists Special Publication 17, p. 221–233.

Davidson, S.K., Hartley, A.J., Weissmann, G.S., Nichols, G.J., and Scuderi, L.A., 2013, Geomorphic elements on modern distributive fluvial systems: Geomorphology, v. 180–181, p. 82–95, https://doi.org/10.1016/j.geomorph.2012.09.008.

DeCelles, P.G., 2011, Foreland basin systems revisited: Variations in response to tectonic settings, *in* Busby, C., and Azor, A., eds., Tectonics of Sedimentary Basins: Recent Advances: Chichester, UK, John Wiley & Sons, p. 405–426.

DeCelles, P.G., and Giles, K.A., 1996, Foreland basin systems: Basin Research, v. 8, no. 2, p. 105–123, https://doi.org/10.1046/j.1365-2117.1996.01491.x.

DeCelles, P.G., and Horton, B.K., 2003, Early to middle Tertiary foreland basin development and the history of Andean crustal shortening in Bolivia: Geological Society of America Bulletin, v. 115, p. 58–77, https://doi.org/10.1130/0016-7606(2003)115<0058:ETMTFB>2.0.CO;2.

DeCelles, P.G., Carrapa, B., Horton, B.K., and Gehrels, G.E., 2011, Cenozoic foreland basin system in the Central Andes of northwestern Argentina: Implications for Andean geodynamics and modes of deformation: Tectonics, v. 30, TC6013, https://doi.org/10.1029/2011TC002948.

Dickinson, W.R., and Gehrels, G.E., 2009, Use of U-Pb ages of detrital zircons to infer maximum depositional ages of strata: A test against a Colorado Plateau Mesozoic database: Earth and Planetary Science Letters, v. 288, p. 115–125, https://doi.org/10.1016/j.epsl.2009.09.013.

Dickinson, W.R., Beard, L.S., Brakenridge, G.R., Erjavec, J.L., Ferguson, R.C., Inman, K.F., Knepp, R.A., Lindberg, F.A., and Ryberg, P.T., 1983, Provenance of North American Phanerozoic sandstones in relation to tectonic settings: Geological Society of America Bulletin, v. 94, p. 222–235, https://doi.org/10.1130/0016-7606(1983)94<222:PONAPS>2.0.CO;2.

Echavarría, L., Hernández, R., Allmendinger, R.W., and Reynolds, J., 2003, Subandean thrust and fold belt of northwestern Argentina: Geometry and timing of the Andean evolution: American Association of Petroleum Geologists Bulletin, v. 87, no. 6, p. 965–985, https://doi.org/10.1306/01200300196.

Fisher, R.V., and Schmincke, H.U., 1984, Pyroclastic Rocks and Tectonic Environment, *in* Pyroclastic rocks: Berlin Heidelberg, Springer, p. 383–409, https://doi.org/10.1007/978-3-642-74864-6_14.

Fosdick, J.C., Carrapa, B., and Ortíz, G., 2015, Faulting and erosion in the Argentine Precordillera during changes in subduction regime: Reconciling bedrock cooling and detrital records: Earth and Planetary Science Letters, v. 432, p. 73–83, https://doi.org/10.1016/j.epsl.2015.09.041.

Fosdick, J.C., Reat, E.J., Carrapa, B., Ortiz, G., and Alvarado, P.M., 2017, Retroarc basin reorganization and aridification during Paleogene uplift of the southern central Andes: Tectonics, v. 36, no. 3, p. 493–514, https://doi.org/10.1002/2016TC004400.

Gehrels, G., 2014, Detrital zircon U-Pb geochronology applied to tectonics: Annual Review of Earth and Planetary Sciences, v. 42, p. 127–149, https://doi.org/10.1146/annurev-earth-050212-124012.

Gehrels, G., and Pecha, M., 2014, Detrital zircon U-Pb geochronology and Hf isotope geochemistry of Paleozoic and Triassic passive margin strata of western North America: Geosphere, v. 10, p. 49–65, https://doi.org/10.1130/GES00889.1.

Giambiagi, L., Tunik, M.A., and Ghiglione, M.A., 2001, Cenozoic tectonic evolution of the Alto Tunuyán foreland basin above the transition zone between the flat and normal subduction segment (33°30′–34°S), western Argentina: Journal of South American Earth Sciences, v. 14, no. 7, p. 707–724, https://doi.org/10.1016/S0895-9811(01)00059-1.

Giambiagi, L., Alvarez, P.P., Godoy, E., and Ramos, V.A., 2003a, The control of pre-existing extensional structures on the evolution of the southern sector of the Aconcagua fold and thrust belt, southern Andes: Tectonophysics, v. 369, no. 1, p. 1–19, https://doi.org/10.1016/S0040-1951(03)00171-9.

Giambiagi, L., Ramos, V.A., Godoy, E., Alvarez, P.P., and Orts, S., 2003b, Cenozoic deformation and tectonic style of the Andes, between 33 and 34 south latitude: Tectonics, v. 22, no. 4, p. 1041, https://doi.org/10.1029/2001TC001354.

Giambiagi, L., Tunik, M., Ramos, V., and Godoy, E., 2009, The High Andean Cordillera of central Argentina and Chile along the Piuquenes Pass–Cordón del Portillo transect: Darwin's pioneering observations compared with modern geology: Revista de la Asociación Geológica Argentina, v. 64, no. 1, p. 43–54.

Giambiagi, L., Mescua, J., Bechis, F., Tassara, A., and Hoke, G., 2012, Thrust belts of the southern Central Andes: Along-strike variations in shortening, topography, crustal geometry, and denudation: Geological Society of America Bulletin, v. 124, p. 1339–1351, https://doi.org/10.1130/B30609.1.

Giambiagi, L., Spagnotto, S., Moreiras, S., Gómez, G., Stahlschmidt, E., and Mescua, J., 2015, Three-dimensional approach to understanding the relationship between the Plio-Quaternary stress field and tectonic inversion in the Triassic Cuyo basin, Argentina: Solid Earth, v. 6, p. 1–17.

Gradstein, F.M., Ogg, J.G., and Smith, A.G., 2004, A Geologic Time Scale 2004: Cambridge, UK, Cambridge University Press, 384 p.

Gutscher, M.A., Spakman, W., Bijwaard, H., and Engdahl, E.R., 2000, Geodynamics of flat subduction: Seismicity and tomographic constraints from the Andean margin: Tectonics, v. 19, no. 5, p. 814–833, https://doi.org/10.1029/1999TC001152.

Hampton, B.A., and Horton, B.K., 2007, Sheetflow fluvial processes in a rapidly subsiding basin, Altiplano plateau, Bolivia: Sedimentology, v. 54, p. 1121–1148, https://doi.org/10.1111/j.1365-3091.2007.00875.x.

Hervé, F., 1988, Late Paleozoic subduction and accretion in southern Chile: Episodes, v. 11, no. 3, p. 183–188.

Hoke, G.D., Giambiagi, L.B., Garzione, C.N., Mahoney, J.B., and Strecker, M.R., 2014, Neogene paleoelevation of intermontane basins in a narrow, compressional mountain range, southern Central Andes of Argentina: Earth and Planetary Science Letters, v. 406, p. 153–164, https://doi.org/10.1016/j.epsl.2014.08.032.

Hoke, G.D., Graber, N.R., Mescua, J.F., Giambiagi, L.B., Fitzgerald, P.G., and Metcalf, J.R., 2015, Near pure surface uplift of the Argentine Frontal Cordillera: Insights from (U-Th)/He thermochronometry and geomorphic analysis, *in* Sepúlveda, S.A., Giambiagi, L.B., Moreiras, S.M., Pinto, L., Tunik, M., Hoke, G.D., and Farías, M., eds., Geodynamic Processes in the

Andes of Central Chile and Argentina: Geological Society, London, Special Publication 399, p. 383–399, https://doi.org/10.1144/SP399.4.

Horton, B.K., 1998, Sediment accumulation on top of the Andean orogenic wedge: Oligocene to late Miocene basins of the Eastern Cordillera, southern Bolivia: Geological Society of America Bulletin, v. 110, p. 1174–1192, https://doi.org/10.1130/0016-7606(1998)110<1174:SAOTOT>2.3.CO;2.

Horton, B.K., and DeCelles, P.G., 1997, The modern foreland basin system adjacent to the Central Andes: Geology, v. 25, p. 895, https://doi.org/10.1130/0091-7613(1997)025<0895:TMFBSA>2.3.CO;2.

Horton, B.K., and DeCelles, P., 2001, Modern and ancient fluvial megafans in the foreland basin system of the Central Andes, southern Bolivia: Implications for drainage network evolution in fold-thrust belts: Basin Research, v. 13, no. 1, p. 43–63, https://doi.org/10.1046/j.1365-2117.2001.00137.x.

Horton, B.K., Hampton, B.A., and Waanders, G., 2001, Paleogene synorogenic sedimentation in the Altiplano plateau and implications for initial mountain building in the Central Andes: Geological Society of America Bulletin, v. 113, p. 1387–1400, https://doi.org/10.1130/0016-7606(2001)113<1387:PSSITA>2.0.CO;2.

Horton, B.K., Fuentes, F., Boll, A., Starck, D., Ramírez, S.G., and Stockli, D.F., 2016, Andean stratigraphic record of the transition from backarc extension to orogenic shortening: A case study from the northern Neuquén Basin, Argentina: Journal of South American Earth Sciences, v. 71, p. 17–40, https://doi.org/10.1016/j.jsames.2016.06.003.

Howard, J.L., 1993, The statistics of counting clasts in rudites: A review, with examples from the upper Palaeogene of southern California, USA: Sedimentology, v. 40, no. 2, p. 157–174, https://doi.org/10.1111/j.1365-3091.1993.tb01759.x.

Ingersoll, R.V., Bullard, T.F., Ford, R.L., Grimm, J.P., Pickle, J.D., and Sares, S.W., 1984, The effect of grain size on detrital modes: A test of the Gazzi-Dickinson point counting method: Journal of Sedimentary Petrology, v. 54, p. 103–116.

Irigoyen, M., Buchan, K., and Brown, R., 2000, Magnetostratigraphy of Neogene Andean foreland-basin strata, lat 33 S, Mendoza Province, Argentina: Geological Society of America Bulletin, v. 112, no. 6, p. 803–816, https://doi.org/10.1130/0016-7606(2000)112<803:MONAFS>2.0.CO;2.

Johnson, N.M., Jordan, T.E., Johnsson, P.A., and Naeser, C.W., 1986, Magnetic polarity stratigraphy, age and tectonic setting of fluvial sediments in an eastern Andean foreland basin, San Juan Province, Argentina, *in* Allen, P.A., and Homewood, P., eds., Foreland Basins: Oxford, UK, Blackwell Publishing Ltd., p. 63–75, https://doi.org/10.1002/9781444303810.ch3.

Jordan, T.E., 1995, Retroarc foreland and related basins, *in* Busby, C.J., and Ingersoll, R.V., eds., Tectonics of Sedimentary Basins: Oxford, UK, Blackwell Science, p. 331–362.

Jordan, T.E., and Allmendinger, R.W., 1986, The Sierras Pampeanas of Argentina: A modern analogue of Rocky Mountain foreland deformation: American Journal of Science, v. 286, no. 10, p. 737–764, https://doi.org/10.2475/ajs.286.10.737.

Jordan, T.E., Isacks, B.L., Allmendinger, R.W., Brewer, J.A., Ramos, V.A., and Ando, C.J., 1983, Andean tectonics related to geometry of subducted Nazca plate: Geological Society of America Bulletin, v. 94, p. 341–361, https://doi.org/10.1130/0016-7606(1983)94<341:ATRTGO>2.0.CO;2.

Jordan, T.E., Allmendinger, R.W., Damanti, J.F., and Drake, R.E., 1993, Chronology of motion in a complete thrust belt: The Precordillera, 30–31°S, Andes Mountains: The Journal of Geology, v. 101, no. 2, p. 135–156, https://doi.org/10.1086/648213.

Jordan, T.E., Schlunegger, F., and Cardozo, N., 2001, Unsteady and spatially variable evolution of the Neogene Andean Bermejo foreland basin, Argentina: Journal of South American Earth Sciences, v. 14, p. 775–798, https://doi.org/10.1016/S0895-9811(01)00072-4.

Kay, S.M., and Mpodozis, C., 2002, Magmatism as a probe to the Neogene shallowing of the Nazca plate beneath the modern Chilean flat-slab: Journal of South American Earth Sciences, v. 15, p. 39–57.

Kay, S.M., Ramos, V.A., Mpodozis, C., and Sruoga, P., 1989, Late Paleozoic to Jurassic silicic magmatism at the Gondwana margin: Analogy to the middle Proterozoic in North America?: Geology, v. 17, no. 4, p. 324–328, https://doi.org/10.1130/0091-7613(1989)017<0324:LPTJSM>2.3.CO;2.

Kay, S.M., Godoy, E., and Kurtz, A., 2005, Episodic arc migration, crustal thickening, subduction erosion, and magmatism in the south-central Andes: Geological Society of America Bulletin, v. 117, no. 1–2, p. 67–88, https://doi.org/10.1130/B25431.1.

Kay, S.M., Ramos, V.A., and Dickinson, W.R., editors, 2009, Backbone of the Americas: Shallow Subduction, Plateau Uplift, and Ridge and Terrane Collision: Geological Society of America Memoir 204, 278 p., https://doi.org/10.1130/MEM204.

Kleiman, L.E., and Japas, M.S., 2009, The Choiyoi volcanic province at 34°S–36°S (San Rafael, Mendoza, Argentina): Implications for the late Palaeozoic evolution of the southwestern margin of Gondwana: Tectonophysics, v. 473, no. 3, p. 283–299, https://doi.org/10.1016/j.tecto.2009.02.046.

Kley, J., Monaldi, C.R., and Salfity, J.A., 1999, Along-strike segmentation of the Andean foreland: Causes and consequences: Tectonophysics, v. 301, no. 1–2, p. 75–94, https://doi.org/10.1016/S0040-1951(98)90223-2.

Kocurek, G., 1981, Significance of interdune deposits and bounding surfaces in aeolian dune sands: Sedimentology, v. 28, p. 753–780, https://doi.org/10.1111/j.1365-3091.1981.tb01941.x.

Kocurek, G., and Dott, R.H., Jr., 1981, Distinctions and uses of stratification types in the interpretation of eolian sand: Journal of Sedimentary Petrology, v. 51, p. 579–595.

Levina, M., Horton, B.K., Fuentes, F., and Stockli, D.F., 2014, Cenozoic sedimentation and exhumation of the foreland basin system preserved in the Precordillera thrust belt (31–32°S), southern central Andes, Argentina: Tectonics, v. 33, no. 9, p. 1659–1680, https://doi.org/10.1002/2013TC003424.

Ludwig, K., 2012, User's Manual for Isoplot Version 3.75–4.15: A Geochronological Toolkit for Microsoft Excel: Berkeley Geochronological Center Special Publication 5, 75 p.

Löbens, S., Sobel, E.R., Bense, F.A., Wemmer, K., Dunkl, I., and Siegesmund, S., 2013, Refined exhumation history of the northern Sierras Pampeanas, Argentina: Tectonics, v. 32, p. 453–472.

Lossada, A.C., Giambiagi, L., Hoke, G.D., Fitzgerald, P.G., Creixell, C., Murillo, I., Mardonez, D., Velásquez, R., and Suriano, J., 2017, Thermochronologic evidence for late Eocene Andean mountain building at 30 S: Tectonics, v. 36, p.2693–2713.

Mahoney, B., Buelow, E.K., Suriano, J., Kimbrough, D., Mescua, J., and Giambiagi, L., 2016, Tracking basin inversion in the retroarc foreland basin: Integrated provenance studies in the Cacheuta basin, south-central Andes, *in* Proceedings of the 35th International Geological Congress: Capetown, South Africa, International Geological Congress, Abstract T29.6:5110.

Mazzitelli, M., Mahoney, B.J., Balgord, E., Giambiagi, L.B., Kimbrough, D., Lossada, A.C., and McCann, C., 2015, Evolution of the Manantiales Basin, San Juan, Argentina: Constraining Miocene orogenic patterns in the south-central Andes: Geological Society of America Abstracts with Programs, v. 47, no. 7, p. 151.

Mescua, J.F., Mahoney, J.B., Suriano, J., Vera, B., Kimbrough, D.L., Giambiagi, L.B., Cerdeño, E., and Buelow, E., 2017, Edad U-Pb de la Formación Divisadero Largo y consideraciones paleoambientales: XX Congreso Geológico Argentino, Actas, v. S9, p. 31–32.

Miall, A.D., 1977, Lithofacies types and vertical profile models in braided river deposits: A summary, *in* Miall, A.D., ed., Fluvial Sedimentology: Canadian Society of Petroleum Geologists Memoir 5, p. 597–604.

Naipauer, M., Tapia, F., Mescua, J., Farías, M., Pimentel, M.M., and Ramos, V.A., 2015, Detrital and volcanic zircon U-Pb ages from southern Mendoza (Argentina): An insight on the source regions in the northern part of the Neuquén Basin: Journal of South American Earth Sciences, v. 64, p. 434–451, https://doi.org/10.1016/j.jsames.2015.09.013.

Nemec, W., and Steel, R.J., 1984, Alluvial and coastal conglomerates: Their significant features and some comments on gravelly mass-flow deposits, *in* Koster, E.H., and Steel, R.J., eds., Sedimentology of Gravels and Conglomerates: Canadian Society of Petroleum Geologists Memoir 10, p. 1–31.

Olsen, H., 1987, Ancient ephemeral stream deposits: A local terminal fan model from the Bunter Sandstone Formation (L. Triassic) in the Tønder-3, -4 and -5 wells, Denmark, *in* Frostick, L., and Reid, I., eds., Desert Sediments: Ancient and Modern: Geological Society, London, Special Publication 35, p. 69–86, https://doi.org/10.1144/GSL.SP.1987.035.01.06.

Ouimet, W.B., and Cook, K.L., 2010, Building the Central Andes through axial lower crustal flow: Tectonics, v. 29, no. 3, TC3010, https://doi.org/10.1029/2009TC002460.

Porras, H., Pinto, L., Tunik, M., Giambiagi, L., and Deckart, K., 2016, Provenance of the Miocene Alto Tunuyán Basin (33°40′S, Argentina) and its implications for the evolution of the Andean Range: Insights from petrography and U-Pb LA-ICPMS zircon ages: Tectonophysics, v. 690, p. 298–317, https://doi.org/10.1016/j.tecto.2016.09.034.

Ramos, V.A., 1999, Plate tectonic setting of the Andean Cordillera: Episodes, v. 22, p. 183–190.

Ramos, V.A., and Folguera, A., 2009, Andean flat-slab subduction through time, *in* Murphy, J.B., Keppie, J.D., and Hynes, A.J., eds., Ancient Orogens and Modern Analogues: Geological Society, London, Special Publication 327, p. 31–54, https://doi.org/10.1144/SP327.3.

Ramos, V.A., Cegarra, M., and Cristallini, E., 1996, Cenozoic tectonics of the High Andes of west-central Argentina (30–36°S latitude): Tectonophysics, v. 259, no. 1, p. 185–200, https://doi.org/10.1016/0040-1951(95)00064-X.

Ramos, V.A., Cristallini, E., and Pérez, D.J., 2002, The Pampean flat-slab of the Central Andes: Journal of South American Earth Sciences, v. 15, no. 1, p. 59–78, https://doi.org/10.1016/S0895-9811(02)00006-8.

Reading, H.G., ed., 1996, Sedimentary Environments: Processes, Facies and Stratigraphy (3rd Ed.): Oxford, Blackwell Science, 704 p.

Rocha-Campos, A., Basei, M., Nutman, A.P., Kleiman, L.E., Varela, R., Llambias, E., Canile, F., and da Rosa, O., 2011, 30 million years of Permian volcanism recorded in the Choiyoi igneous province (W Argentina) and their source for younger ash fall deposits in the Paraná Basin: SHRIMP U-Pb zircon geochronology evidence: Gondwana Research, v. 19, no. 2, p. 509–523, https://doi.org/10.1016/j.gr.2010.07.003.

Sato, A.M., Llambías, E.J., Basei, M.A., and Castro, C.E., 2015, Three stages in the late Paleozoic to Triassic magmatism of southwestern Gondwana, and the relationships with the volcanogenic events in coeval basins: Journal of South American Earth Sciences, v. 63, p. 48–69, https://doi.org/10.1016/j.jsames.2015.07.005.

Siame, L.L., Bellier, O., and Sebrier, M., 2006, Active tectonics in the Argentine Precordillera and western Sierras Pampeanas: Revista de la Asociación Geológica Argentina, v. 61, no. 4, p. 604–619.

Somoza, R., and Ghidella, M.E., 2012, Late Cretaceous to recent plate motions in western South America revisited: Earth and Planetary Science Letters, v. 331–332, p. 152–163, https://doi.org/10.1016/j.epsl.2012.03.003.

Spalletti, L.A., Fanning, M., and Rapela, C.W., 2009, Dating the Triassic continental rift in the southern Andes: The Potrerillos Formation, Cuyo Basin, Argentina: Geologica Acta, v. 6, no. 3, p. 267–283.

Stear, W.M., 1985, Comparison of the bedform distribution and dynamics of modern and ancient sandy ephemeral flood deposits in the southwestern Karoo region, South Africa: Sedimentary Geology, v. 45, no. 3, p. 209–230, https://doi.org/10.1016/0037-0738(85)90003-X.

Steel, R., and Thompson, D., 1983, Structures and textures in Triassic braided stream conglomerates ('Bunter' pebble beds) in the Sherwood Sandstone Group, North Staffordshire, England: Sedimentology, v. 30, no. 3, p. 341–367, https://doi.org/10.1111/j.1365-3091.1983.tb00677.x.

Strecker, M., Cerveny, P., Bloom, A., and Malizia, D., 1989, Late Cenozoic tectonism and landscape development in the foreland of the Andes: Northern Sierras Pampeanas (26–28°S), Argentina: Tectonics, v. 8, no. 3, p. 517–534, https://doi.org/10.1029/TC008i003p00517.

Suriano, J., Mardonez, D., Mahoney, J.B., Mescua, J.F., Giambiagi, L.B., Kimbrough, D., and Lossada, A., 2017, Uplift sequence of the Andes at 30°S: Insights from sedimentology and U/Pb dating of synorogenic deposits: Journal of South American Earth Sciences, v. 75, p. 11–34, https://doi.org/10.1016/j.jsames.2017.01.004.

Tucker, M.E., 2011, Sedimentary Rocks in the Field: A Practical Guide: New York, John Wiley & Sons, 288 p.

Uba, C.E., Heubeck, C., and Hulka, C., 2005, Facies analysis and basin architecture of the Neogene Subandean synorogenic wedge, southern Bolivia: Sedimentary Geology, v. 180, no. 3, p. 91–123, https://doi.org/10.1016/j.sedgeo.2005.06.013.

Walcek, A.A., and Hoke, G.D., 2012, Surface uplift and erosion of the southernmost Argentine Precordillera: Geomorphology, v. 153–154, p. 156–168, https://doi.org/10.1016/j.geomorph.2012.02.021.

Walker, R.G., 1992, Facies, facies models and modern stratigraphic concepts, *in* Walker, R.G., and James, N.P., eds., Facies Models: Response to Sea Level Change: St. Johns, Newfoundland, Geological Association of Canada, p. 1–14.

Yáñez, G. A., Ranero, C. R., Huene, R., and Díaz, J., 2001, Magnetic anomaly interpretation across the southern Central Andes (32–34°S): The role of the Juan Fernández Ridge in the Late Tertiary evolution of the margin: Journal of Geophysical Research–Solid Earth (1978–2012), v. 106, no. B4, p. 6325–6345.

Yrigoyen, M.R., 1993, Revisión estratigráfica del neógeno de la región Cacheuta–La Pilona–Tupungato, Mendoza septentrional, Argentina, *in* Proceedings XII Congreso Geológico Argentino y II Congreso de Exploración de Hidrocarburos, Mendoza, Argentina: Asociación Geológica Argentina (AGA) and Instituto Argentino del Petróleo y del Gas (IAPG), Actas, v. 2, p. 187–199.

Zapata, T.R., and Allmendinger, R.W., 1996, Growth stratal records of instantaneous and progressive limb rotation in the Precordillera thrust belt and Bermejo Basin, Argentina: Tectonics, v. 15, p. 1065–1083, https://doi.org/10.1029/96TC00431.

MANUSCRIPT RECEIVED 2 OCTOBER 2017
REVISED MANUSCRIPT RECEIVED 3 JANUARY 2018
MANUSCRIPT ACCEPTED 31 JANUARY 2018